Cell

Decidual NK Cells Transfer Granulysin to Selectively Kill Bacteria in Trophoblasts

Graphical Abstract

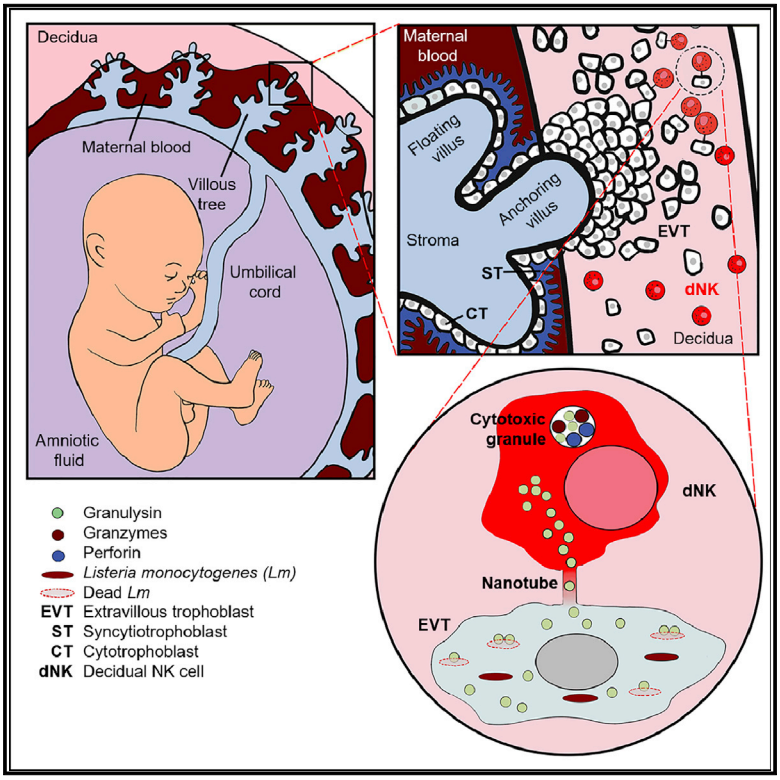

Highlights

- Decidual NK cells kill *Listeria* in trophoblasts without killing the placental cells
- Decidual NK cells selectively transfer granulysin to trophoblasts without degranulating
- Granulysin transfer occurs through nanotube connections
- A *GNLY* transgene protects *Listeria*-infected mice from spontaneous abortion

Authors

Ângela C. Crespo, Sachin Mulik, Farokh Dotiwala, ..., Tamara Tilburgs, Jack L. Strominger, Judy Lieberman

Correspondence

tamara.tilburgs@cchmc.org (T.T.), jlstrom@fas.harvard.edu (J.L.S.), judy.lieberman@childrens.harvard.edu (J.L.)

In Brief

Natural killer cells fend off *Listeria* infection in the placenta by funneling an antimicrobial peptide through nanotubes to infected trophoblasts.

Crespo et al., 2020, Cell *182*, 1125–1139
September 3, 2020
https://doi.org/10.1016/j.cell.2020.07.019

Cell

CellPress

Article

Decidual NK Cells Transfer Granulysin to Selectively Kill Bacteria in Trophoblasts

Ângela C. Crespo,[1,2,3,8] Sachin Mulik,[1,5,8] Farokh Dotiwala,[1,6] James A. Ansara,[1] Sumit Sen Santara,[1] Kayleigh Ingersoll,[1] Cristian Ovies,[1] Caroline Junqueira,[1,4] Tamara Tilburgs,[2,7,*] Jack L. Strominger,[2,*] and Judy Lieberman[1,9,*]

[1]Program in Cellular and Molecular Medicine, Boston Children's Hospital and Department of Pediatrics, Harvard Medical School, Boston, MA 02115, USA

[2]Department of Stem Cell and Regenerative Biology, Harvard University, Cambridge, MA 02138, USA

[3]PhD Programme in Experimental Biology and Biomedicine, Center for Neurosciences and Cell Biology, University of Coimbra, 3004-504 Coimbra, Portugal

[4]Instituto René Rachou, Fundação Oswaldo Cruz, Belo Horizonte, MG 30190-009, Brazil

[5]Present address: Department of Pulmonary Immunology, Center for Biomedical Research, The University of Texas Health Science Center at Tyler, Tyler, TX 75708, USA

[6]Present address: Vaccine and Immunotherapy Center, The Wistar Institute, Philadelphia, PA 19104, USA

[7]Present address: Division of Immunobiology and Center for Inflammation and Tolerance, Cincinnati Children's Hospital, and Department of Pediatrics, University of Cincinnati College of Medicine, Cincinnati, OH 45229 USA

[8]These authors contributed equally

[9]Lead Contact

*Correspondence: tamara.tilburgs@cchmc.org (T.T.), jlstrom@fas.harvard.edu (J.L.S.), judy.lieberman@childrens.harvard.edu (J.L.)

https://doi.org/10.1016/j.cell.2020.07.019

SUMMARY

Maternal decidual NK (dNK) cells promote placentation, but how they protect against placental infection while maintaining fetal tolerance is unclear. Here we show that human dNK cells highly express the antimicrobial peptide granulysin (GNLY) and selectively transfer it via nanotubes to extravillous trophoblasts to kill intracellular *Listeria monocytogenes* (*Lm*) without killing the trophoblast. Transfer of GNLY, but not other cell death-inducing cytotoxic granule proteins, strongly inhibits *Lm* in human placental cultures and in mouse and human trophoblast cell lines. Placental and fetal *Lm* loads are lower and pregnancy success is greatly improved in pregnant *Lm*-infected *GNLY*-transgenic mice than in wild-type mice that lack *GNLY*. This immune defense is not restricted to pregnancy; peripheral NK (pNK) cells also transfer GNLY to kill bacteria in macrophages and dendritic cells without killing the host cell. Nanotube transfer of GNLY allows dNK to protect against infection while leaving the maternal-fetal barrier intact.

INTRODUCTION

Decidual natural killer (dNK) cells, the most abundant immune cells at the maternal-fetal interface in the first trimester of pregnancy, are prime candidates for protection against placental infection. dNK cells are armed to kill; they express high levels of the cytolytic effectors perforin (PFN), granzymes (Gzms), and granulysin (GNLY) (King et al., 1993; Koopman et al., 2003; Vujaklija et al., 2011). However, they do not kill classical NK target cells as well as peripheral NK (pNK) cells (Hanna et al., 2006; Koopman et al., 2003; Kopcow et al., 2005; Moffett-King, 2002). Although dNK cells kill human cytomegalovirus (HCMV)-infected decidual (maternal) stromal cells, they do not degranulate or kill (fetal) extravillous trophoblasts (EVTs) even when they are infected (Crespo et al., 2016; Siewiera et al., 2013). Thus, the maternal immune response in the placenta is handicapped for defense against infection.

Fetal and maternal cells contact each other at the villi, where maternal blood bathes villous trophoblast (VT) syncytia for nutrient exchange and the maternal decidua, where EVTs anchor the villi to the uterus (Moffett-King, 2002). VT syncytia resist some bacterial infections, whereas EVTs have heightened susceptibility and can be infected by a variety of pathogens (Cao and Mysorekar, 2014; Robbins et al., 2010). Maternal infection can be transmitted by trophoblasts and spread to the fetus with severe consequences. *In utero* infection with viruses (Zika, HCMV, other herpesviruses, rubella, and B19 parvovirus), bacteria (*Listeria monocytogenes* [*Lm*], group B streptococci [GBS], and syphilis), and parasites (*Toxoplasma gondii* and *Plasmodium* spp.) causes fetal distress and loss, premature labor, congenital anomalies, and intrauterine growth restriction (Błaszkowska and Góralska, 2014; Zeldovich and Bakardjiev, 2012).

dNK cell tolerance of infected VTs and EVTs contributes to pathogen persistence and promotes fetal transmission. Tolerance has been linked to special properties of trophoblasts (Hanna et al., 2006; Kopcow et al., 2005; Moffett-King, 2002). VTs do not express classical major histocompatibility complex (MHC) class I (to avoid T cell recognition) or known NK cell-activating ligands. EVTs only express human leukocyte antigen (HLA)-C and nonclassical MHC molecules, including HLA-E and -G, which are

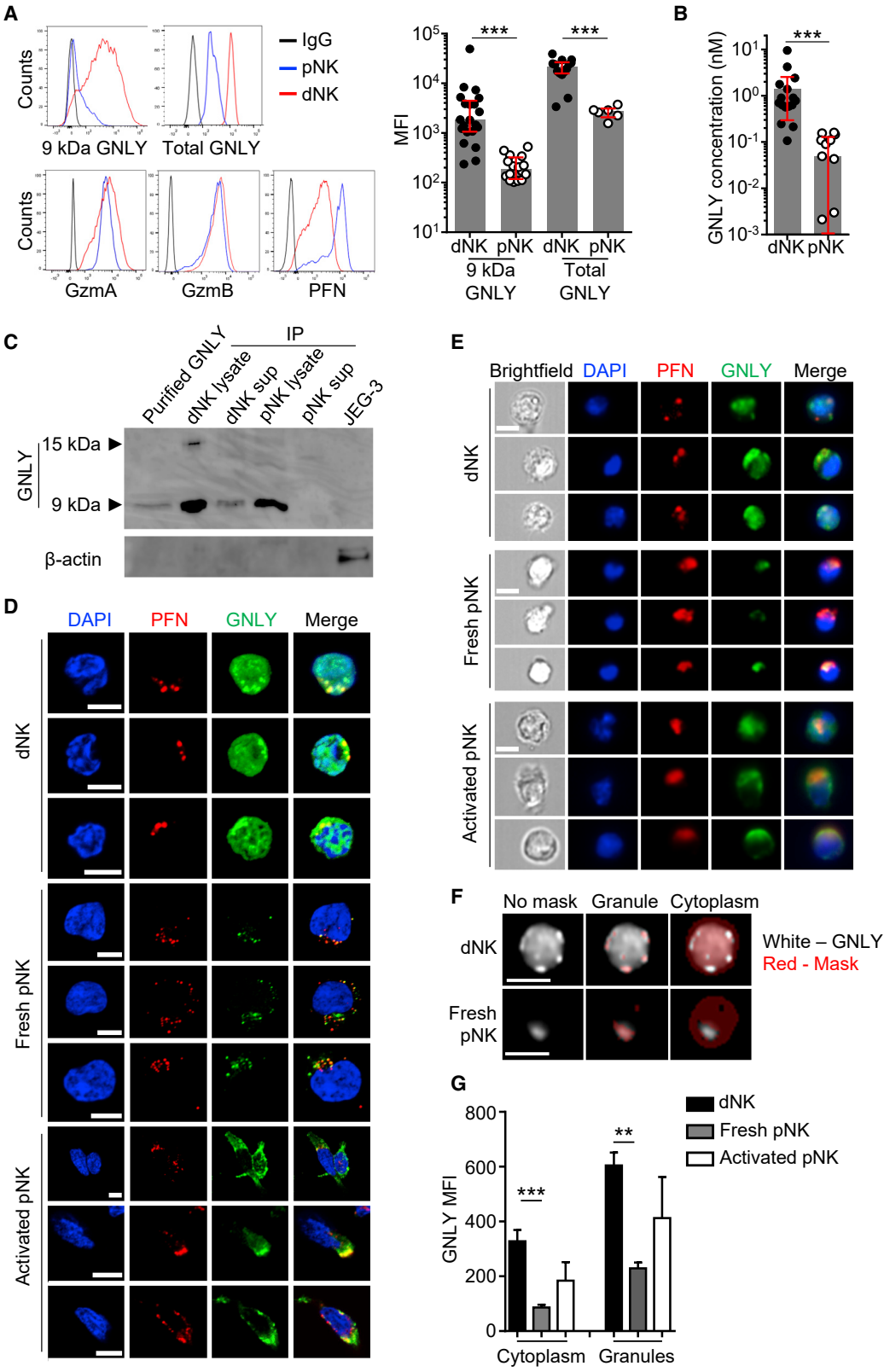

(legend on next page)

recognized by inhibitory and activating NK cell receptors. The molecular basis for reduced dNK cell cytotoxicity is not well understood. dNK cells secrete cytokines, such as interleukin-8 (IL-8), vascular endothelial growth factor (VEGF), and granulocyte-macrophage-colony stimulating factor (GM-CSF), that increase trophoblast migration, uterine spiral artery remodeling, placentation, and uterine vascularization (Hanna et al., 2006; Koopman et al., 2003), and regulation of trophoblast invasion and differentiation to promote placentation is considered the main role of dNK cells. The tolerogenic placental environment favors fetal and placental development (Crespo et al., 2017; Erlebacher, 2013; Zeldovich and Bakardjiev, 2012) but interferes with immune defense.

GNLY, an antimicrobial peptide expressed only by killer lymphocytes, selectively disrupts bacterial, fungal, and parasite membranes (Dotiwala and Lieberman, 2019). GNLY is proteolytically processed from a 15-kDa precursor to a 9-kDa active protein. Most mammals, but not rodents, express GNLY. The other cytotoxic granule pore-forming protein, PFN, selectively injures mammalian but not microbial membranes. Ordinarily, when a killer cell recognizes an infected cell, cytotoxic granules move to the immune synapse and release their cytotoxic granule proteins into the synapse (Walch et al., 2014). PFN delivers GNLY and Gzms into the infected host cell, where the Gzms kill the host cell. Within the target, GNLY delivers the Gzms into intracellular microbes to trigger microptosis—programmed cell death in microbes (Dotiwala et al., 2016, 2017; Walch et al., 2014). Thus, killer cell-mediated death of intracellular microbes requires all three cytotoxic effector molecules: PFN, Gzms, and GNLY. At high concentrations, GNLY on its own lyses bacteria, but at lower concentrations, bacterial killing depends on Gzms (Dotiwala et al., 2016; Stenger et al., 1998; Walch et al., 2014).

dNK cells express more GNLY than pNK cells and secrete GNLY constitutively (Vujaklija et al., 2011). However, the role of GNLY in dNK cell defense against placental infection has not been studied. To investigate whether dNK cell GNLY helps protect against intrauterine infection in pregnancy, we studied *Lm* infection. *Lm* spreads to the placenta either via an ascending vaginal infection or from the blood. Pregnant women have 17-fold more clinically symptomatic *Lm* infection than the general population. *Lm* can cause miscarriage, stillbirth, preterm delivery, and neonatal sepsis. Here we describe how dNK cells balance the contradictory demands of tolerating fetal cells and protecting against infection. dNK cells kill intracellular *Lm* in trophoblasts without killing the infected trophoblasts. GNLY and cell-cell connections via nanotubes are involved.

RESULTS

dNK Cells Highly Express GNLY in Cytotoxic Granules and the Cytosol

dNK cells from healthy first-trimester decidua express GNLY and other cytolytic granule proteins (PFN, GzmA, and GzmB), as reported previously (Crespo et al., 2016; King et al., 1993; Vujaklija et al., 2011; Figures 1A and S1A). dNK cells contain ten times more 9-kDa and total GNLY than healthy donor pNK cells, as assessed using DH2 and RB1 monoclonal antibodies, respectively. PFN was about ten times lower in dNK cells than pNK cells, consistent with their reduced cytotoxicity against mammalian cells. After overnight culture in a low amount of IL-15 (2.5 ng/mL), dNK cells constitutively secreted ~20-fold more GNLY than pNK cells (Figure 1B). Only the active form was secreted (Figure 1C). dNK cells secreted significantly less GzmA, GzmB, and PFN than GNLY (Figure S1B). Because GNLY was secreted selectively compared with other cytotoxic granule components, GNLY and PFN localization in dNK cells was compared. By confocal microscopy (Figures 1D and S1C) and imaging flow cytometry (Figures 1E–1G, S1D, and S1E), two pools of dNK cell GNLY were visualized: in cytotoxic granules and in the cytosol. In contrast, PFN was only in granules. In fresh pNK cells, GNLY staining was dimmer and localized with PFN in cytotoxic granules. In pNK cells activated for 6 days with 5 ng/mL IL-15 and 50 U/mL IL-2, GNLY expression increased but was still lower than in dNK cells and was in the cytoplasm and granules. Thus, when GNLY expression is high in dNK cells or activated pNK cells, it localizes to cytotoxic granules and the cytosol, whereas PFN is restricted to cytotoxic granules.

dNK Cells Kill *Lm* in a Trophoblast-like Cell Line without Degranulating or Killing Trophoblasts

To investigate whether the high amounts of secreted 9-kDa GNLY kill bacteria, dNK and pNK cell supernatants were added to cell-free *Lm* or to an *Lm*-infected trophoblast-like choriocarcinoma cell line, JEG-3 (Apps et al., 2009; Figure 2A). dNK but not pNK cell supernatants reduced cell-free *Lm* colony-forming units (CFUs) by 2-fold. However, neither supernatant reduced *Lm* CFUs in JEG-3 cells. Next, the ability of dNK and pNK cells to kill intracellular *Lm* in JEG-3 cells was tested. 3-h coculture with dNK or pNK cells significantly reduced intracellular *Lm* CFUs in JEG-3 cells (Figure 2B, left). Surprisingly, dNK and pNK cells did not kill JEG-3 cells (Figure 2B, right) or release their cytotoxic granules, as assessed by externalization of CD107a,

Figure 1. dNKs Express GNLY within Cytotoxic Granules and in the Cytosol

(A) Representative flow cytometry histograms (left) of GNLY (9 kDa [clone DH2] and total [clone RB1]), GzmA, GzmB, and PFN and mean fluorescence intensity (MFI) (right) of GNLY staining of human dNK and pNK cells.

(B) GNLY in 12-h culture supernatants of human dNK (n = 18) and pNK (n = 13) cells by ELISA.

(C) Representative immunoblot, probed with GNLY polyclonal rabbit antisera, of purified GNLY or GNLY immunoprecipitated (IP) with clone DH10 (which recognizes 9-kDa and 15-kDa GNLY) from dNK or pNK cell lysates or supernatants (sup). JEG-3 cell lysate is a negative control.

(D) Confocal images of representative dNK, fresh pNK, and activated pNK cells stained for total GNLY (RB1) and PFN, acquired with a Zeiss LSM 700 microscope. Scale bars, 5 μm.

(E) Representative raw images from imaging flow cytometry of NK cells stained for total GNLY (RB1), PFN, and DAPI. Scale bars, 7 μm.

(F and G) Examples of cytoplasmic and granule masks (F) used to measure GNLY localization (G). Scale bars, 7 μm. Cytoplasmic and granule GNLY MFIs were measured in 1,000–6,000 cells from 3–5 donors by imaging flow cytometry.

Data show median with interquartile range (A and B) or mean ± SEM (G). $^{**}p < 0.01$, $^{***}p < 0.001$ by Mann-Whitney rank test or Kolmogorov-Smirnov test (A and B) or unpaired one-way ANOVA, followed by Tukey's post-test of each cell type compared with every other type (G). See also Figures S1A–S1E.

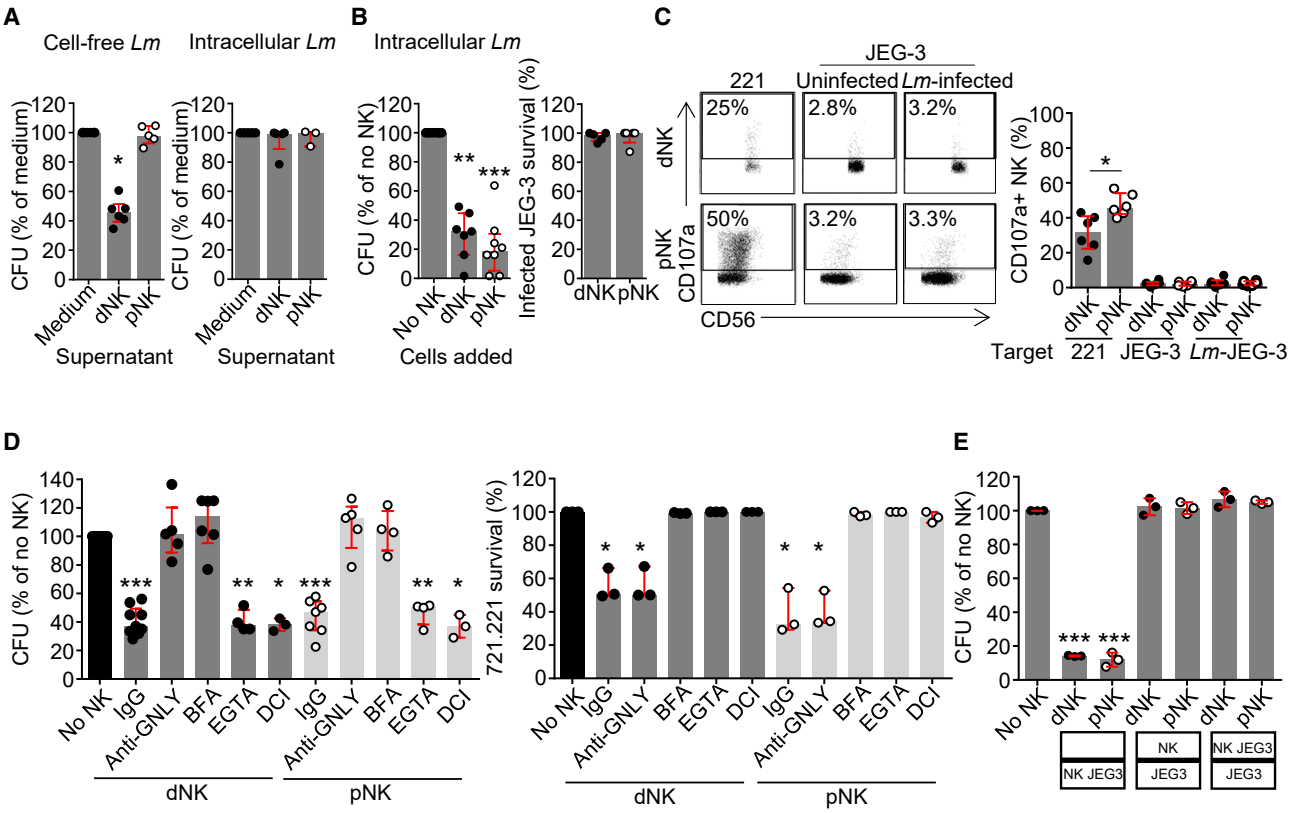

Figure 2. NK Cells Kill *Lm* in a Trophoblast-like Cell Line without Killing the Host Cell

(A) Cell-free *Lm* (left) or *Lm* CFUs in infected JEG-3 cells (right) after 3-h culture with medium or supernatants from dNK or pNK cell overnight cultures.

(B) Intracellular CFUs (left) and JEG-3 cell viability (right), normalized to medium control samples, after 3-h coincubation of *Lm*-infected JEG-3 cells with medium or dNK or pNK cells (effector:target [E:T] ratio, 10:1).

(C) Representative dNK and pNK cell flow cytometry dot plots (left) and percentage of NK cells with externalized CD107a (right) after 4-h incubation with 721.221 (221) or uninfected or *Lm*-infected JEG-3 cells.

(D) Intracellular CFUs in *Lm*-infected JEG-3 cells (left) and 721.221 viability (right) after incubation with dNK or pNK cells that were pretreated with anti-GNLY or control immunoglobulin G (IgG), BFA, EGTA, or DCI. Antibodies and EGTA were also present during the co-culture.

(E) Intracellular CFUs in *Lm*-infected JEG-3 cells in the bottom chamber after co-culture for 12 h with dNK or pNK cells in the same chamber or separated by a Transwell membrane. CFUs were normalized to control (Ctrl) samples without NK cells.

Shown is median with interquartile range. *$p < 0.05$, **$p < 0.01$, ***$p < 0.001$ by non-parametric unpaired one-way ANOVA (Kruskal-Wallis test) (A; B, left; D; and E) followed by Dunn's post-tests comparing each NK cell type with medium (A and B, left), or treatment in pNK or dNK cells with untreated control (no NK) (D and E) and Kolmogorov-Smirnov test (B, right, and C). See also Figure S1F.

during co-culture with uninfected or *Lm*-infected JEG-3 cells (Figure 2C). In contrast, dNK and pNK cells degranulated and killed 721.221, a conventional NK cell target (Figure 2C, D right). *Lm* suppression without host cell death is a potential mechanism to establish immunity without breaking placental immune tolerance.

To understand how bacteria are suppressed without killing the host cell, dNK and pNK cells were pre-incubated overnight with anti-GNLY (clone DH10) or an isotype control antibody and then co-cultured with *Lm*-infected JEG-3 cells in the continued presence of antibody. Incubation with the GNLY-blocking antibody, which was internalized by dNK and JEG-3 cells during overnight co-culture (Figure S1F), blocked bacterial killing by dNK or pNK cells (Figure 2D, left). Pre-incubation of dNK and pNK cells with brefeldin A (BFA), which blocks transport of secreted proteins from the endoplasmic reticulum (ER) to the Golgi apparatus and loading of cytotoxic granules, and its continued presence in the culture medium during coculture also completely prevented bacterial killing. However, EGTA, which blocks degranulation and PFN pore formation, or 3,4-dichloroisocoumarin (DCI), a pan-Gzm inhibitor, did not reduce killing of *Lm* in JEG-3 cells (Figure 2D, left). Thus, killing of intracellular *Lm* depends on GNLY but occurs independent of degranulation, PFN, and Gzms. In contrast, and as expected, dNK and pNK cell killing of 721.221 was blocked by BFA, EGTA, and DCI but not by anti-GNLY (Figure 2D, right), consistent with cytotoxic granule-mediated killing of 721.221. To determine whether direct cell contact was required to kill intracellular *Lm*, dNK and pNK cells were cocultured with *Lm*-infected JEG-3 cells while separated or not by a Transwell membrane. Bacteria were not killed when dNK or pNK cells were separated from *Lm*-infected JEG-3 cells (Figure 2E). To

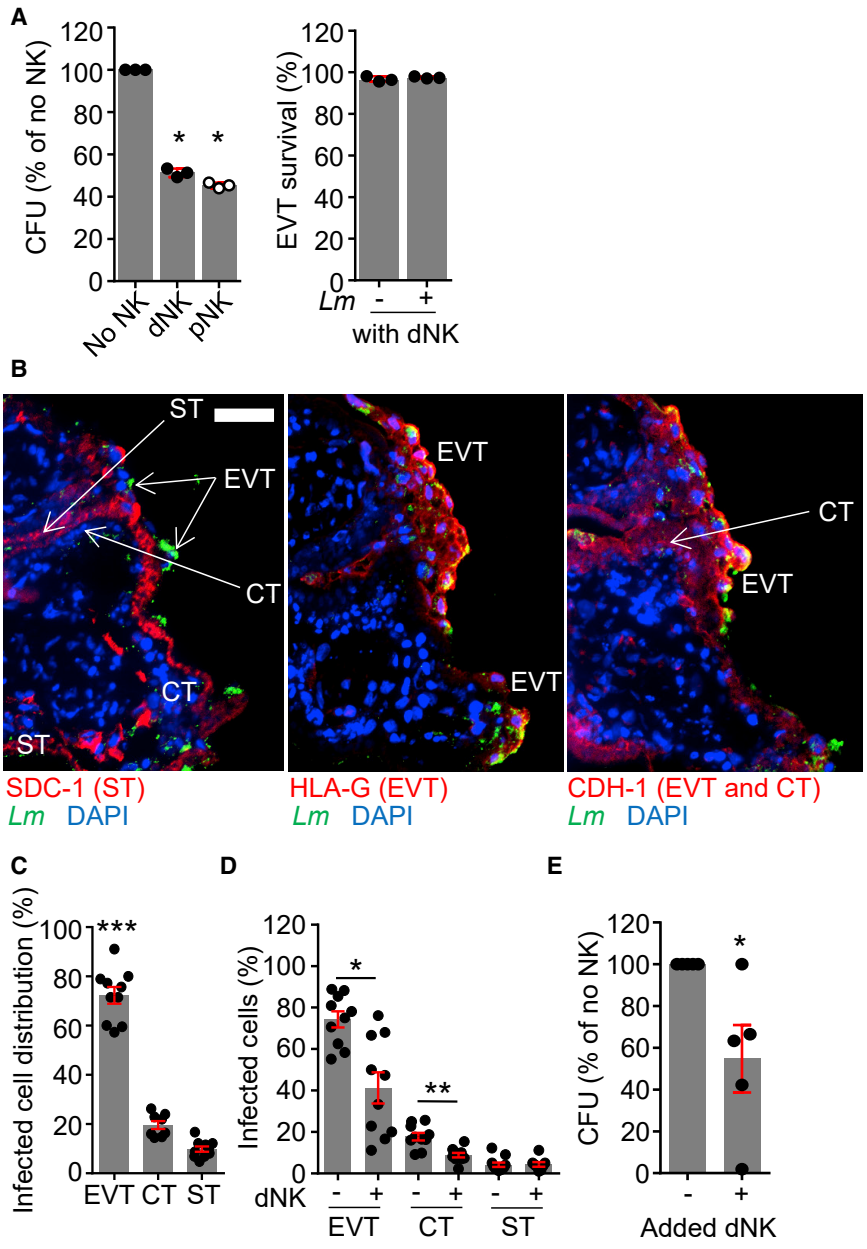

Figure 3. dNK Cells Kill *Lm* in 1° Trophoblasts *In Vitro* and in 3D Villous Cultures *In Situ*

(A) Intracellular CFUs in HLA-G$^+$ EVTs (left) and EVT survival (right) after co-culture with dNK cells, pNK cells, or medium for 3 h.

(B) Representative immunofluorescence images of three consecutive 5-μm cryosections of a placental villous tree infected with *Lm* and stained for DAPI, *Lm*, SDC-1 (an ST marker, left), HLA-G (an EVT marker, center), and E-cadherin (CDH-1; an CT and EVT marker, right), acquired with an Axio Observer spinning disk confocal microscope. Cell types were identified by staining, nuclear size, and localization. Scale bar, 50 μm.

(C) Distribution of *Lm*-infected cells among trophoblast cell types 72 h after infection of villous explants.

(D) Percentage of infected EVTs, CTs, and STs in villi cultured with or without autologous dNK cells or medium for 72 h.

Percentages in (C) and (D) were calculated in 10 imaging fields (217× magnification) from a representative donor.

(E) *Lm* CFUs in villous cultures incubated for 72 h with dNK cells or medium. For each donor sample, CFUs were normalized to the tissue size estimated by DNA quantification, and CFUs in dNK cell samples were normalized to samples without added NK cells.

Shown is median ± interquartile range (A) or mean ± SEM (C–E). *p < 0.05, **p < 0.01, ***p < 0.001 by unpaired non-parametric one-way ANOVA (Kruskal-Wallis test followed by Dunn's post-test (A, left, comparing cells co-cultured with and without NK cells), Wilcoxon rank test (A, right), one-way ANOVA followed by Tukey's post-test comparing each cell type with each other (C), and paired t test (D and E).

determine whether cell contact might only be necessary to activate dNK cell secretion of GNLY, which could then be taken up by cells in the bottom chamber, we exposed dNK cells to infected JEG-3 cells in the top insert and measured killing of intracellular *Lm* in JEG-3 cells in the bottom of the Transwell (Figure 2E, last lane). Bacteria were not killed in the separated infected JEG-3 cells. Therefore, dNK and pNK cell killing of intracellular *Lm* requires cell contact.

dNK Cells Kill *Lm* in 1° EVTs without Killing the EVTs

To verify that the results obtained with JEG-3 cells hold for 1° EVTs, isolated 1° EVTs were infected with *Lm* before co-culture with dNK or pNK cells. pNK and dNK cells significantly reduced intracellular *Lm* CFU in 1° EVTs but did not kill the EVTs (Figure 3A). To investigate whether dNK cells suppress *Lm* infection in primary tissue, 3D placental villous explants that maintain the structure and tissue distribution of placental cells, prepared as described (Rizzuto et al., 2016; Robbins et al., 2010), were infected with *Lm* for 72 h. Infection mostly occurred in HLA-G$^+$ CDH-1$^+$ cells with large nuclei located at the tips of the villi, which identified them as EVTs (Figures 3B–3D), confirming previous reports that EVTs are the main *Lm*-infected placental cells (Cao and Mysorekar, 2014; Robbins et al., 2010). Cytotrophoblasts (CTs; cells with small nuclei located under EVTs or syncytium and identified by CDH-1 expression) made up ~20% of the remaining infected cells. *Lm* was rarely seen in stromal cells or syncytiotrophoblasts (STs; identified as SDC-1$^+$ cells with small nuclei in a continuous layer surrounding the villi), consistent with a previous report that STs are resistant to infection (Robbins et al., 2010). About 80% of EVTs were infected, whereas only ~20% of CTs and a small percentage of STs were infected. CT

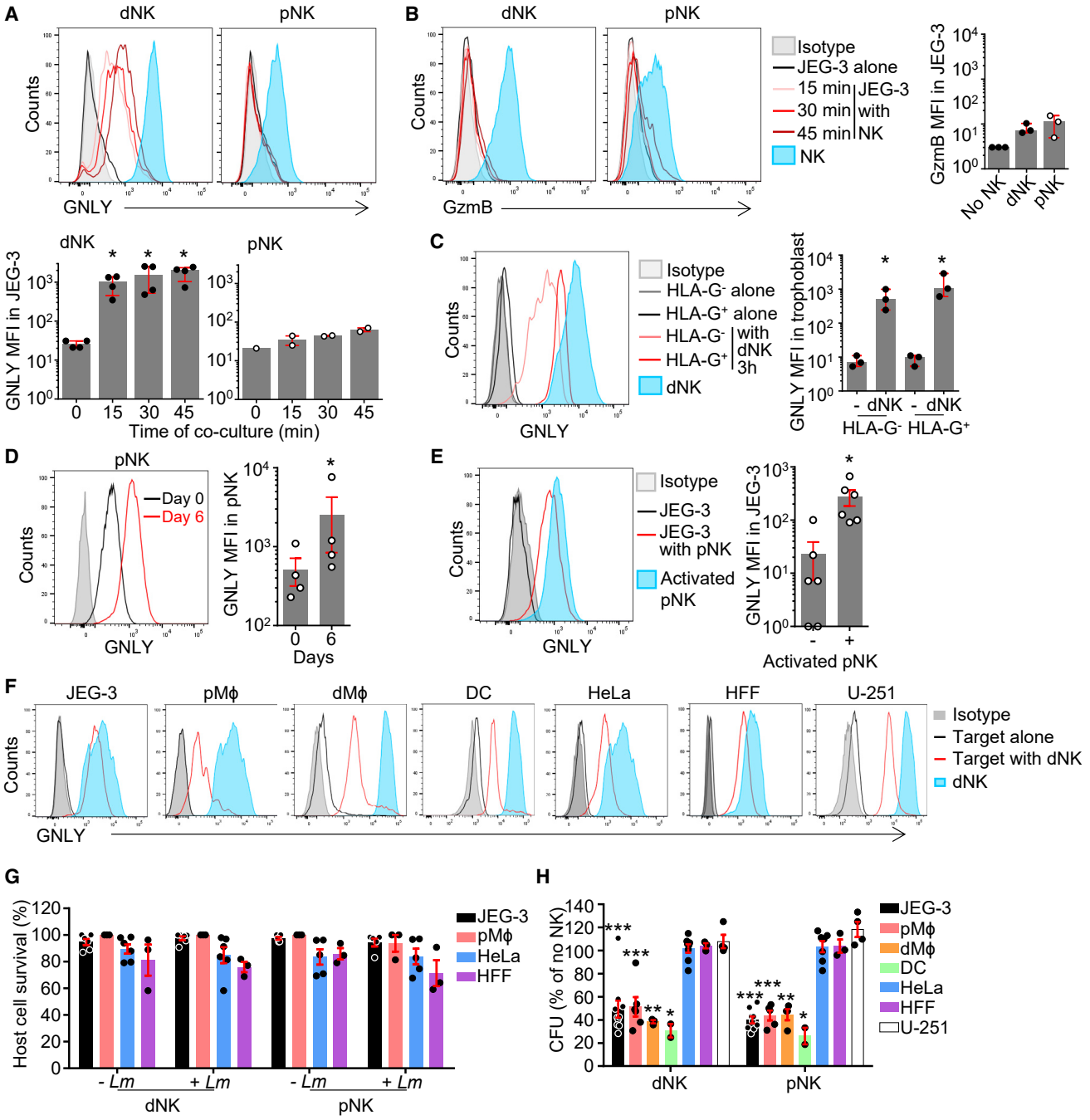

Figure 4. dNK Cells Transfer GNLY, but not GzmB, into JEG-3 Cells and 1° Trophoblasts

(A) Representative flow cytometry histograms (top) and GNLY MFI (bottom) in NK or JEG-3 cells cultured without or with dNK or pNK cells for the indicated times.

(B) Representative flow cytometry histograms (left) of GzmB in NK or JEG-3 cells cultured without or with dNK or pNK cells for the indicated times. A graph (right) shows GzmB MFI in JEG-3 cells after coculture for 45 min.

(C) Representative flow cytometry histograms of dNK cells and isolated human 1° trophoblasts (a mixture of HLA-G$^+$ EVTs and HLA-G$^-$ STs and CTs) cultured with or without dNK cells for 3 h (left) and GNLY MFI in trophoblasts after 3-h culture with dNK or pNK cells (right).

(D) Representative flow cytometry histogram (left) and GNLY MFI (right) in freshly isolated pNK cells and after 6 days of cytokine activation.

(E) Representative flow cytometry histogram *(left)* and GNLY MFI *(right)* in activated pNK and JEG-3 cultured without or with activated pNK.

(F) Flow cytometry histograms of intracellular GNLY in dNK cells or the indicated target cells cultured for 3 h with or without dNK cells (data are representative of 3 dNK cell samples.)

(G and H) Host cell viability (G) and mean change in intracellular *Lm* CFU (H) when *Lm*-infected cells were incubated for 3 h with dNK or pNK cells from 3–5 donors or medium.

(legend continued on next page)

infection may have been partly a culture artifact because some of the syncytial layer, which forms a barrier to infection, was eroded in the tissue slices (Robbins et al., 2010). When dNK cells were added to *Lm*-infected villous explants for 72 h, the overall bacterial burden, as assessed by CFUs, was reduced 2-fold (Figure 3E). The number of infected trophoblasts of each subtype counted in stained tissue slices revealed a similar decline in infected EVTs and CTs in the presence of dNK cells (Figure 3D). Thus, dNK cells kill intracellular *Lm* and significantly reduce the bacterial load in primary cells and tissues. However, dNK cells do not kill 1° EVTs even when they are infected.

dNK Cells Deliver GNLY, but Not GzmB, into Trophoblasts

The cell contact and GNLY dependence of bacterial killing suggest that NK cells directly transfer GNLY to JEG-3 cells. To investigate this possibility, JEG-3 cells were incubated for 5–45 min with no NK cells or a 10-fold excess of dNK or pNK cells and stained for intracellular GNLY (Figures 4A and S2A) and GzmB (Figure 4B). Within 10 min of dNK cell co-culture, JEG-3 cells stained strongly for intracellular GNLY but not for GzmB. After 3 h of dNK:JEG-3 cell co-culture, JEG-3 cells became almost as bright as donor dNK cells (GNLY mean fluorescence intensity (MFI) of JEG-3 cells, 2,850 ± 1,130 versus dNK cells, 3,430 ± 912; Figure S2B). During dNK cell co-culture for 3 h with autologous 1° trophoblasts, GNLY was detected in HLA-G$^-$ VTs and HLA-G$^+$ EVTs (Figure 4C). (In these experiments cells were trypsinized before staining to guarantee that the detected GNLY was intracellular.) In contrast, GNLY and GzmB were not detected in JEG-3 cells after co-culture with pNK cells, even after 3 h (Figure S2B). However, cytokine-activated pNK cells, which express significantly more GNLY than freshly isolated pNK cells (Figures 1G and 4D), transferred detectable amounts of GNLY to JEG-3 cells after 1 h of coculture (Figure 4E). dNK cell transfer of GNLY to uninfected and *Lm*-infected JEG-3 cells was comparable (Figure S2C), suggesting that GNLY transfer is constitutive. Thus, dNK cells efficiently and selectively transfer GNLY, but not GzmB, to JEG-3 cells and 1° EVTs, whereas pNK cell transfer to JEG-3 cells becomes detectable only when pNK cell GNLY is increased.

NK Cells Transfer Small Dyes to JEG-3 Cells

To determine whether transfer was specific for GNLY, JEG-3 cells were co-cultured with a 10-fold excess of dNK or pNK cells stained with carboxyfluorescein succinimidyl ester (CFSE) (a cytosolic dye) or DiO (a membrane dye), and dye transfer was evaluated by flow cytometry. dNK and pNK cells transferred CFSE and DiO to JEG-3 cells as early as 15 min (Figures S2D and S2E). The amount of dye in JEG-3 cells increased with time and correlated with the amount of dye in the NK cells (activated pNK cells > dNK cells > fresh pNK cells). However, when JEG-3 cells were loaded with CFSE or DiO, no dye was transferred from JEG-3 cells to NK cells (Figures S2F and S2G). Thus, transfer was unidirectional from NK to JEG-3 cells in the 3-h time period studied. However, transfer of cell-surface HLA-G from EVTs to dNK cells by trogocytosis has been observed with longer incubation (Tilburgs et al., 2015a).

dNK Cells Transfer GNLY and Kill Intracellular *Lm* in Macrophages and Dendritic Cells

To assess whether dNK cells transfer GNLY to other cell types, dNK cells were co-cultured for 3 h with uninfected human 1° blood monocyte-derived macrophages, decidual macrophages, THP-1 cells differentiated into dendritic cells (DCs), human foreskin fibroblasts (HFFs), HeLa cells, and U-251 glioblastoma cells and stained for intracellular GNLY (Figure 4F). dNK cells efficiently transferred GNLY to all of these cells, but transfer was greatest to HFFs. dNK or pNK cells did not kill these cells when they were infected with *Lm* (Figure 4G). However, dNK and pNK cells reduced bacterial colonies in JEG-3 cells, 1° blood monocyte-derived macrophages, decidual macrophages, and DCs but, surprisingly, not in HFFs, HeLa cells, or U-251 cells, even though all of these cells internalized GNLY during dNK cell co-culture (Figure 4H). Bacterial killing did not correlate with the efficiency of GNLY transfer. To begin to understand why transferred GNLY kills bacteria only in some cells, GNLY localization with bacteria was compared by confocal microscopy in cells in which bacteria were killed (JEG-3 cells and 1° blood monocyte-derived macrophages) or not killed (HeLa cells and HFFs) (Figure S3). GNLY co-localized significantly more with fluorescently labeled *Lm* in cells in which bacteria were killed, suggesting that differences in GNLY or bacterial trafficking may determine whether bacteria are killed. Further work is needed to understand why GNLY localization and bacterial killing differ among infected target cells.

NK Cells Form Nanotubes to Trophoblasts that Transfer GNLY

In previous studies, GNLY transfer and cytotoxic lymphocyte-mediated killing of infected target cells occurred at the immune synapse after granule exocytosis and depended on PFN (Dotiwala et al., 2016; Walch et al., 2014). However, NK killing of *Lm* within JEG-3 cells and EVTs is unusual because it is contact-dependent but independent of PFN, Gzms, or degranulation (Figures 2 and 3). To probe the mechanism of transfer, contacts between dNK and pNK cells with *Lm*-infected or uninfected JEG-3 cells or 721.221 were visualized using confocal microscopy 45–60 min after co-culture. Slides were fixed and stained for GNLY, PFN, LFA-1 (expressed by NK cells but not JEG-3 cells or 721.221), and actin (Figures S4A–S4E). LFA-1 and actin rearranged at the immune synapse. dNK and pNK cells formed LFA-1-capped immune synapses with 721.221 (Figures S4C and S4D). In most of these conjugates, cytotoxic granules localized to the point of contact (Figure S4E). However, significantly fewer dNK than pNK cell immune synapses had polarized granules, consistent with previous reports (Kopcow et al., 2005; Tilburgs et al., 2015a). dNK and pNK cells did not form classical

In all experiments, the E:T ratio was 10:1. Graphs show median ± interquartile range (A–C) or mean ± SEM (D, E, G, and H). *p < 0.05, **p < 0.01, ***p < 0.001 by paired non-parametric one-way ANOVA (Friedman's test followed by Dunn's post-test comparing each time point with time 0 (A), unpaired non-parametric one-way ANOVA (Kruskal-Wallis followed by Dunn's post-test of each NK cell type compared with no NK cells (B), each target with NK cells compared with sample without NK cells (G and H), Wilcoxon rank-sum test (C), and paired t test (D and E). See also Figures S2 and S3.

immune synapses or polarize granules to uninfected or infected JEG-3 cells (Figures S4A, S4B, S4D, and S4E). Remarkably, cytoplasmic extensions, which stained for actin and LFA-1, connected both types of NK cells to JEG-3 cells, more frequently from dNK than pNK cells (Figures S4A and S4B). These structures resemble nanotubes (also called cytoplasmic bridges, tunneling nanotubes, or cytonemes), described previously to connect NK and T cells with target cells (Chauveau et al., 2010; Davis and Sowinski, 2008; Önfelt et al., 2004; Sowinski et al., 2008). The proportion of contacting dNK cells that formed visible nanotubes with JEG-3 cells was similar regardless of whether the cells were infected (data not shown). No nanotubes were seen between dNK or pNK cells and 721.221.

To better visualize dNK cell and JEG-3 cell or EVT connections, super-resolution confocal microscopy with structured illumination (SIM) was used to image slides stained for LFA-1, GNLY, actin, and DAPI (Figures 5A and 5B). With higher resolution, GNLY was observed within nanotubes connecting dNK cells to JEG-3 cells and EVTs. GNLY was also visible in the trophoblast cytoplasm (Figures 5A, center row, and 5B, bottom row). Because the structured illumination algorithm preferentially enhances high-intensity signals, to simultaneously visualize GNLY in nanotubes and the more diffuse GNLY signal in target cells, we also acquired images with a Zeiss Airyscan 880 microscope (Figure S4G). When dNK cells were incubated with JEG-3 cells or 1° EVTs, GNLY was simultaneously detected being transferred to target cells in nanotubes and in the target cell. Control JEG-3 cells or EVTs, cultured without dNK cells, did not stain for GNLY (Figure S4F; see also Figures 4, S2, and S3). To determine the origin of the nanotubes, cocultured CellTracker-labeled JEG-3 cells and DiO-labeled dNK cells were stained with CD49f, expressed only by JEG-3 cells, and CD56, expressed only by dNK cells (Figure 6A). All nanotubes stained along their length for DiO, and only a minority stained with CellTracker or CD49f, suggesting that nanotubes mostly originated from dNK cells. In some JEG-3 cells, transferred DiO was detected, but no transferred CellTracker was detected in dNK cells, consistent with unidirectional transfer seen by flow cytometry (Figures S2D–S2G). When this experiment was repeated with 1° EVTs, dNK cells formed nanotubes with 1° EVTs that stained along their length with DiO (Figure 6B). Videomicroscopy of cocultured DiO-labeled dNK and JEG-3 cells confirmed dNK cell nanotube formation in real time (Videos S1 and S2). Although some nanotube connections were fleeting, some were more sustained. Thus, dNK cells form GNLY-staining nanotube connections, suggesting GNLY transfer from NK cells to trophoblasts via nanotubes.

GNLY Transfer and Bacterial Killing Depend on Actin

Nanotubes lack known specific markers (other than actin) and cannot be inhibited except nonspecifically by inhibiting the actin cytoskeleton. All NK-JEG-3 cell connections stained for F-actin, and about a third also stained for tubulin, consistent with our identification of them as nanotubes (Figure 6C). To verify the role of nanotubes in GNLY transfer, the effect of inhibitors of actin polymerization (cytochalasin D), endocytosis (Dynasore), and microtubules (nocodazole) on GNLY transfer from dNK to JEG-3 cells was assessed (Figures 6D–6F and S5A–S5C). Cells were mixed and centrifuged at 4°C to bring them into close contact before adding inhibitors (except for Dynasore, which was pre-added only to JEG-3 cells). The number of cell contacts with connecting nanotubes and GNLY transfer were reduced significantly by cytochalasin D after 15 min of contact, but Dynasore had no effect, suggesting that the actin cytoskeleton, but not endocytosis, was required for nanotube formation and GNLY transfer (Figures 6D and 6E, left). Importantly, neither inhibitor reduced cell contacts (Figure 6E, right). Because cytochalasin was toxic for JEG-3 cells in longer incubation, the incubation time could not be extended. Pre-incubation of NK cells with cytochalasin D, but not pre-incubation of JEG-3 cells with Dynasore, completely rescued viable bacteria inside JEG-3 cells co-cultured for 3 h with dNK or pNK cells (Figure 6F), further supporting the role of actin in GNLY transfer and bacterial killing. Nocodazole significantly reduced GNLY transfer in the first 15 min of contact, but not after 3 h, and also had no effect on the frequency of contacts, nanotube formation between dNK and JEG-3 cells, or *Lm* viability within NK cell-cocultured JEG-3 cells (Figure S5A–S5C). Thus, the actin cytoskeleton, but not microtubules or endocytosis, mediates GNLY transfer and suppression of intracellular infection, providing additional support for GNLY transfer via actin-dependent nanotubes. Moreover, because inhibiting endocytosis had no effect on bacterial killing or GNLY transfer, uptake of secreted GNLY does not contribute significantly to intracellular bacterial killing.

Neuraminidase Treatment of JEG-3 Cells Inhibits Nanotubes, GNLY Transfer, and Bacterial Killing

Because inhibiting the cytoskeleton affects cell movement and many functions, identifying cell surface receptor-ligand pairs used to make nanotube connections could help to understand how nanotubes are formed. To identify such receptors, JEG-3 or dNK cells were incubated with blocking antibodies to cell surface receptors before and during co-culture: integrins (CD49f [ITGα6], CD104 [ITGβ4], CD11a [LFA-1], and CD58 [LFA-3]), integrin ligand CD2, CD324 (E-cadherin), NK cell receptors (NKG2A, KIR2DL, and LILRB1), HLA (HLA-A,-B,-C and G), CD43, CD45, and Siglec-7 (Koopman et al., 2003; Tilburgs et al., 2015b). None of the antibodies tested individually inhibited GNLY transfer (data not shown). Because some immune receptors use sialic acid for binding (Crocker et al., 2007), pre-incubation with neuraminidase was also assessed. Neuraminidase treatment of JEG-3 but not dNK cells significantly reduced GNLY transfer (Figure S5D) and the frequency of nanotube connections (Figure S5E, left) without affecting dNK:JEG-3 cell contacts (Figure S5E, right). Neuraminidase treatment of *Lm*-infected JEG-3 cells just before adding NK cells increased bacterial CFU 3- to 4-fold (Figures S5F and S5G). Thus, NK cell recognition of sialylated JEG-3 cell ligands promotes nanotube formation, GNLY transfer, and control of intracellular *Lm*.

GNLY-Tg Mice Are Resistant to *Lm*-Induced Spontaneous Abortion

Because mice do not express GNLY, *GNLY*-Tg mice can be used to evaluate the *in vivo* role of GNLY during *Lm* infection in pregnancy. *GNLY*-Tg mice selectively express GNLY in killer lymphocytes at levels comparable with humans (Huang et al.,

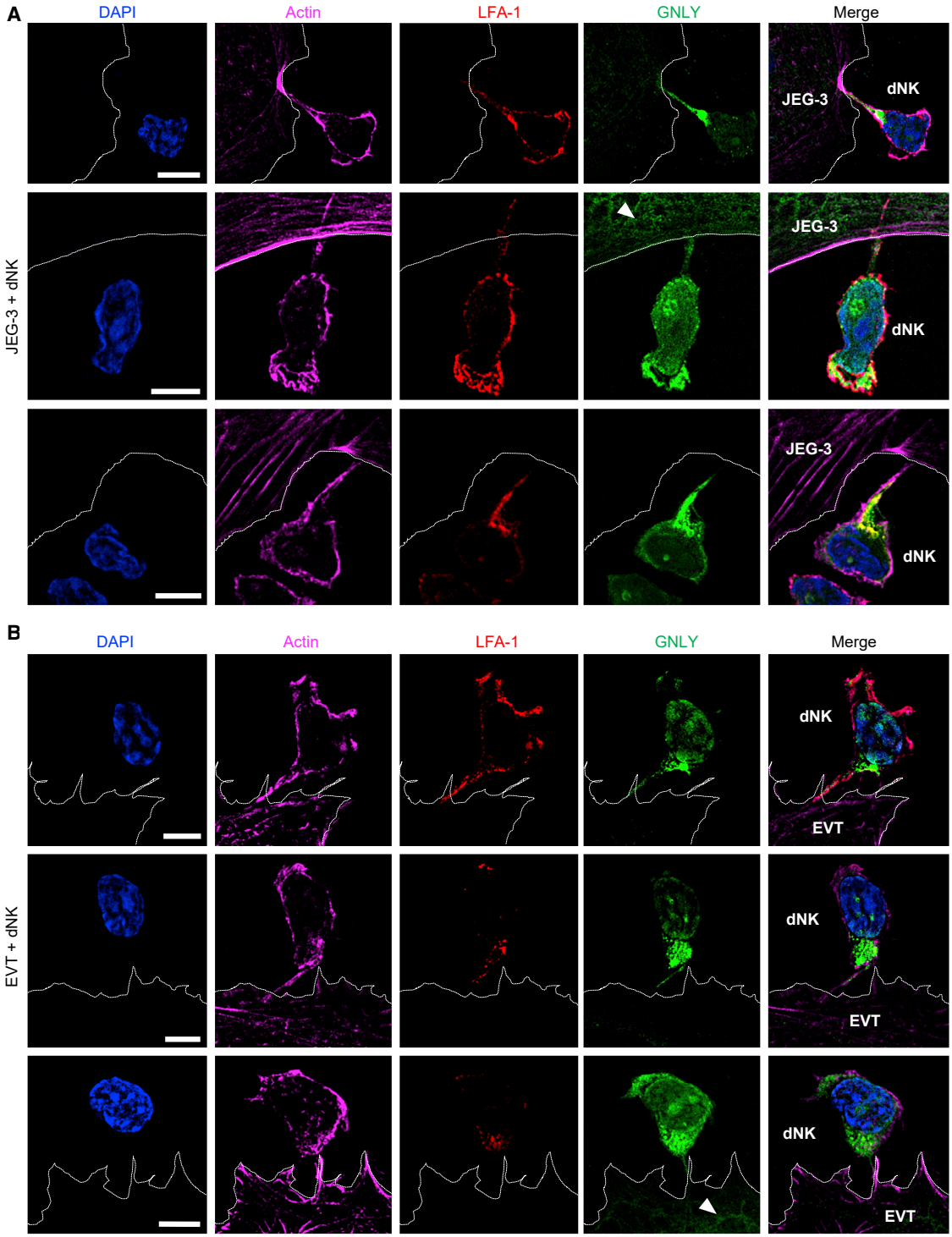

Figure 5. NK Cells Form Nanotubes to JEG-3 Cells and EVTs that Contain GNLY

(A and B) Representative single-channel SIM images showing GNLY (RB1, green) in the cytoplasmic connections (actin, magenta) between dNK and JEG-3 cells (A) or 1° EVTs (B). Images were fixed after 60-min co-culture and acquired with a Zeiss ELYRA microscope. LFA-1 (red) is only expressed in dNK cells. JEG-3 cell and EVT membranes are outlined in white. Arrows indicate GNLY in the target cell. Scale bars, 5 μm. See also Figure S4.

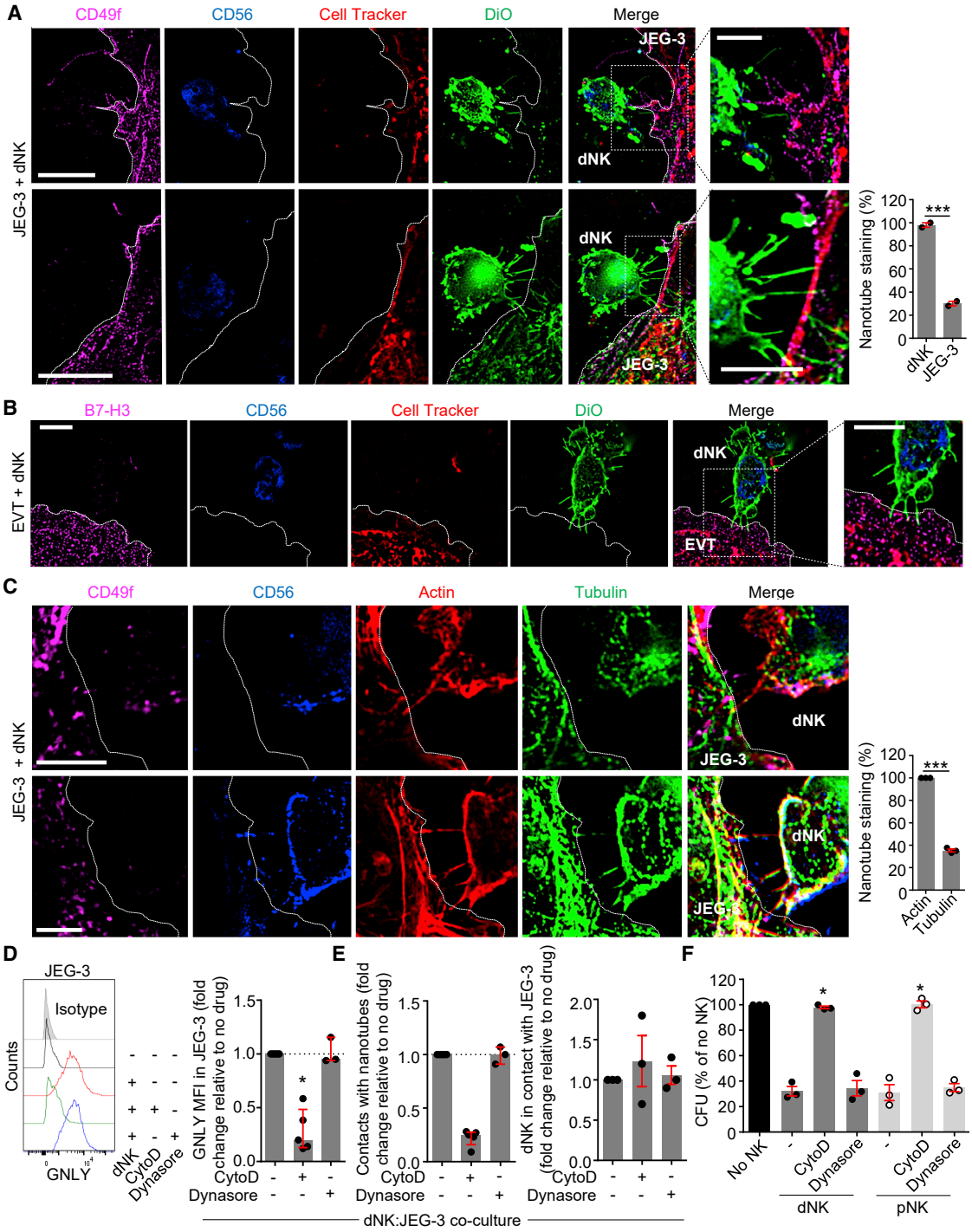

Figure 6. Nanotubes Originate from dNK Cells and Transfer GNLY in an Actin-Dependent Manner

(A) Representative single-channel SIM images of DiO-labeled dNK cells co-cultured with CellTracker Deep Red-labeled JEG-3 cells and stained for CD56 (a dNK cell marker) and CD49f (JEG-3 cell integrin). The top panel shows membrane projections originating from both cells, whereas the bottom panel shows projections only from dNK cells. Scale bars, 10 μm. The JEG-3 cell membrane is delineated. Shown on the right is mean ± SEM percentage of membrane projections staining with DiO (dNK cells) or CD49f (JEG-3 cells) from analysis of 25 contacts in each of 2 donors.

(B) Representative single-channel SIM images of CellTracker-labeled 1° EVTs co-cultured with DiO-labeled dNK cells stained for CD56 and B7-H3 (an EVT marker, magenta). Scale bar, 5 μm. The EVT membrane is outlined.

(C) Representative single-channel SIM images of dNK cells co-cultured for 1 h with JEG-3 cells, stained for CD56 (dNK cells), CD49f (JEG-3 cells), actin, and tubulin. In the bottom panel, tubulin and actin stain the nanotubes, and in the top panel only actin. The JEG-3 cell membrane is delineated. Scale bars, 5 μm.

(legend continued on next page)

2007). As in humans, uterine NK (uNK) cells were abundant in the mouse pregnant uterus (Manaster and Mandelboim, 2010), and a high proportion of *GNLY*-Tg uNK cells and splenic NK (sNK) cells, isolated on gestation day (g.d.) 10, stained for GNLY (Figure 7A). uNK cells, but not sNK cells, from *GNLY*-Tg mice secreted GNLY into culture supernatants at similar levels as human dNK cells (Figures 7B and 1B). As expected, uNK and sNK cells from *GNLY*-Tg and WT mice comparably killed the NK cell target YAC-1 (Figure 7C). Although uNK cells did not kill the mouse trophoblast cell line SM9-1 (Rasmussen et al., 1999), uNK and sNK cells from *GNLY*-Tg, but not from wild-type (WT), mice, significantly reduced intracellular *Lm* CFUs in infected SM9-1 cells, confirming that *Lm* killing by mouse NK cells requires GNLY (Figure 7D). To determine whether PFN contributes to antibacterial activity against *Lm*, uNK cells were isolated from *Prf1*$^{-/-}$ WT and *GNLY*-Tg BALB/c mice. As expected, uNK cells from *Prf1*$^{-/-}$ WT and *GNLY*-Tg mice did not kill YAC-1 or *Lm*-infected SM9-1 cells (Figures S6A and S1B). However, *Prf1*$^{-/-}$*GNLY*-Tg uNK cells reduced *Lm* colonies in SM9-1 cells as well as PFN-sufficient *GNLY*-Tg uNK cells (Figure S6C). Thus, mouse uNK and sNK cells, like human dNK and pNK cells, control intracellular bacteria *in vitro* in a GNLY-dependent but PFN-independent manner without killing the host trophoblast.

To investigate whether GNLY enhances immune protection early in pregnancy, sublethal *Lm* infection on g.d. 6 was compared in pregnant WT and *GNLY*-Tg BALB/c mice. All pregnant WT mice had high bacterial counts in the spleen and liver 3 days after infection ($\sim 10^4$ CFUs/g) (Figure 7E). In contrast, bacteria were not detected in the spleen and liver of about a third of *GNLY*-Tg mice. In mice that had detectable bacteria, CFUs were more than ten times lower than in WT mice. Similarly, bacterial loads were significantly lower in the placentas and fetuses of *GNLY*-Tg than WT mice (Figure 7E). Most importantly, 6 of 10 *GNLY*-Tg dams carried their pregnancies to term and had normal numbers of healthy-appearing pups, whereas 10 of 11 WT dams had failed pregnancies ($p = 0.013$; Figure 7F). Thus, the *GNLY* transgene strongly improves pregnancy outcome after *Lm* infection.

To assess which lymphocytes contribute to *Lm* resistance, bacterial loads and pregnancy outcomes in WT and *GNLY*-Tg mice, depleted or not of NK, CD4, or CD8 T cells (Figure S6D), were compared after *Lm* challenge on g.d. 6. In WT and *GNLY*-Tg mice, depletion of NK cells, but not CD4$^+$ or CD8$^+$ cells, significantly increased bacterial loads 3 days later in all tissues analyzed (Figure S6E). As expected, *GNLY*-Tg mice treated with a control antibody were protected from *Lm*-induced abortion; 6 of 11 *GNLY*-Tg but only 1 of 7 WT mice gave birth to normal litters (Figure 7G). Depletion of NK or CD8$^+$ cells, but not CD4$^+$ cells, led to *Lm*-induced resorption in all *GNLY*-Tg mice, indicating that NK and CD8 T cells contribute to protecting the fetus (Figure 7G). Thus, GNLY in killer lymphocytes significantly reduces bacterial loads in pregnant *GNLY*-Tg mice and protects mice from *Lm*-induced resorption.

DISCUSSION

Here we show that dNK cells transfer GNLY to fetal cells, killing intracellular *Lm* without killing the host cell. This is an unexpected way to protect the placenta from intracellular infection. GNLY transfer occurs independent of cytotoxic granules by nanotubes, which connect the cytosols of two cells through an undefined mechanism. When in the host cell, GNLY traffics to and kills bacteria, presumably by disrupting their cell membranes. GNLY transfer strongly inhibits *Lm* in 1° human EVTs, human 3D villous explants, and mouse and human trophoblast cell lines. Pregnant *GNLY*-Tg mice handled *Lm* infection better than *GNLY*-deficient WT mice and gave birth to normal litters. However, dNK cells only partially control infection, presumably because GNLY on its own is less effective than protection by cytotoxic granules. Cytotoxic granules deploy PFN and Gzms to kill the host cell, removing a favorable niche for *Lm* replication. The combination of Gzms and GNLY kills bacteria more potently because together they not only damage the cell membrane but also disrupt essential bacterial electron transport, protein synthesis, and central metabolism pathways (Dotiwala et al., 2016, 2017; Walch et al., 2014). Nonetheless, GNLY-mediated protection without PFN significantly reduced bacterial loads in all *in vitro* and *in vivo* experiments. Importantly, GNLY provides an immune defense mechanism that avoids rejection of placental trophoblasts and is thus compatible with maintenance of maternal-fetal immune tolerance. Because GNLY broadly disrupts microbial membranes (Zheng et al., 2007; Dotiwala et al., 2016; Stenger et al., 1998; Walch et al., 2014), it may also protect placental and fetal tissues against other bacterial, fungal, and parasite pathogens.

Most experiments were performed using a choriocarcinoma cell line (JEG-3) as a model for EVTs because 1° human trophoblast yields are limited. Although JEG-3 may not be a perfect surrogate (Tilburgs et al., 2015b), it is the only cell line that mimics EVT MHC expression (Apps et al., 2009), which is critical for NK cell interactions. Importantly, our key results (killing of intracellular bacteria without killing the host cell and GNLY transfer via nanotubes) were verified using human 1° EVTs and 3D villous explant cultures. In placental explants, EVTs were the main cell type infected with *Lm*, but dNK cells suppressed *Lm* replication

Shown on the right is mean ± SEM percentage of nanotubes staining for actin or tubulin from analysis of 20–45 contacts in each of 3 donors. All co-cultures lasted 1 h. Images were acquired with a Zeiss ELYRA microscope.

(D) Representative flow cytometry histograms (left) and (median ± interquartile range) fold change in GNLY MFI in JEG-3 cells after culture for 15 min with NK cells (E:T ratio, 3:1) from 3–5 donors in the presence or absence of cytochalasin D (cytoD) or Dynasore.

(E) Effect of inhibitors on the percentage of dNK:JEG-3 cell interactions with visible nanotube connections (left) and the percentage of NK cells in contact with JEG-3 cells (right) after 15 min co-culture. Shown is the fold change compared with no inhibitors (mean ± SEM). For each condition, at least 24 dNK:JEG-3 cell contacts per donor in 3–5 donors were analyzed.

(F) Effect of inhibitors on NK cell suppression of intracellular *Lm* CFUs in JEG-3 cells after 3-h co-culture. Shown are mean ± SEM of percentages relative to culture without NK cells in 3 donors. *$p < 0.05$, **$p < 0.01$, ***$p < 0.001$, by χ^2 test (A, C, and E), paired non-parametric one-way ANOVA (Friedman's test) followed by Dunn's post-test comparing each treatment with no inhibitor (D), and unpaired non-parametric one-way ANOVA (Kruskal-Wallis test) followed by Dunn's post-test, comparing each treatment with no inhibitor (F). See also Figure S5.

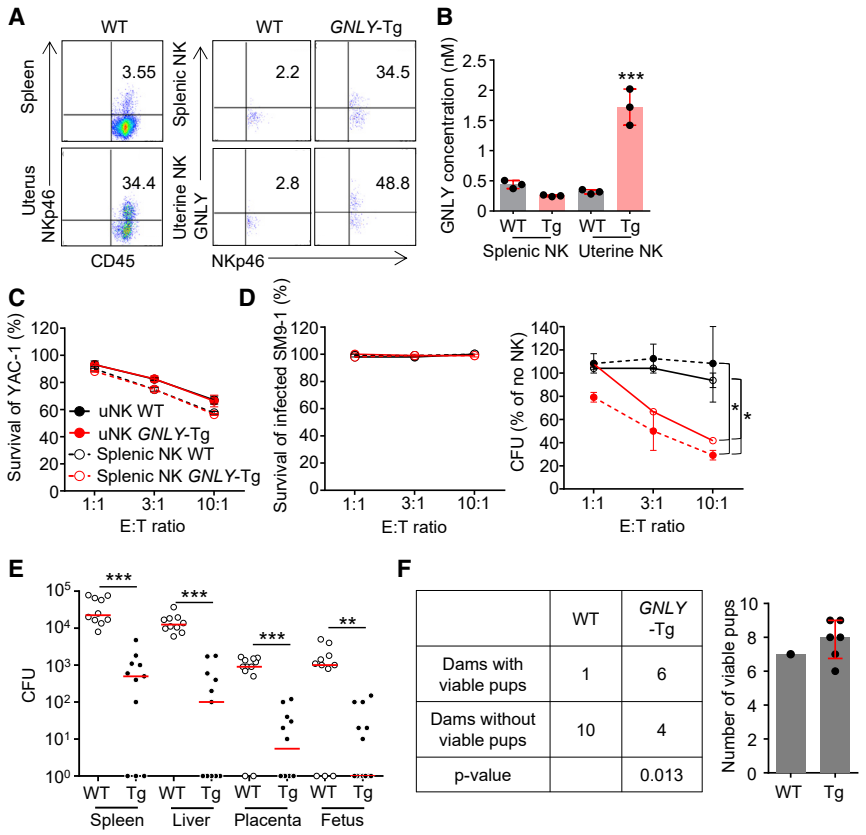

	WT	GNLY -Tg
Dams with viable pups	1	6
Dams without viable pups	10	4
p-value		0.013

G

	WT				GNLY-Tg			
Depletion	Ctrl	NK	CD4	CD8	Ctrl	NK	CD4	CD8
Dams with viable pups	1	0	0	0	6	0	5	0
Dams without viable pups	6	6	5	6	5	9	5	10
p-value		ns	ns	ns		0.008	ns	0.006

Figure 7. *GNLY*-Tg Mouse NK Cells Kill Intracellular Bacteria without Killing a Mouse Trophoblast Cell Line and Protect *GNLY-Tg* Dams from Abortion after *Lm* Infection

(A) Flow cytometry dot plots showing the percentage of murine splenic NK (sNK) cells and uterine NK (uNK) cells within CD45$^+$ cells (left) and the percentage of NK cell staining for GNLY (clone RB1) (right). Data are representative of 3 mice analyzed on g.d. 10.

(B) Secreted GNLY in WT and *GNLY*-Tg mice (n = 3) sNK and uNK cell 12-h culture sups.

(C and D) Viability of YAC-1 (C) and *Lm*-infected SM9-1 (left) and intracellular *Lm* CFUs in SM9-1 (right) (D) after 3-h co-culture with sNK or uNK cells from WT or *GNLY*-Tg animals (n = 3).

(E and F) Bacterial CFUs on g.d. 9 (E) and dams with live pups (left) and mean number of pups per litter in mice that had viable pups (right) (F) in WT (n = 10) and *GNLY*-Tg (n = 11) mice that were infected with *Lm* on g.d. 6.

(G) Pregnancy outcome in WT and *GNLY*-Tg mice depleted of lymphocyte subsets using Ctrl antibody or NK, CD4, or CD8 cell-depleting antibodies (starting at g.d. 3) and then infected with *Lm* on g.d. 6. Depletion was verified on g.d. 6 (Figure S6D).

A χ^2 test compared pregnancy outcome in WT and *GNLY*-Tg mice (F) or in depleted mice, with mice treated with the Ctrl antibody (G). Shown are mean ± SEM (B–D and F). Red lines in (E) represent median values. ns, not significant. *p < 0.05, **p < 0.01, ***p < 0.001 by unpaired one-way ANOVA (B) or unpaired non-parametric one-way ANOVA (Kruskal-Wallis test, C and D) followed by post-tests comparing each NK cell type in each mouse group with every other group (B) and areas under the curve (C and D) and Mann-Whitney or Kolmogorov-Smirnov test (comparing WT with *GNLY*-Tg for each tissue, E). See also Figure S6.

in EVTs and CTs. Human samples varied in the extent of dNK cell suppression of *Lm*, suggesting that genetic or environmental variations affect this immune response.

This study focused on *Lm* infection in early pregnancy, when dNK cells are the main decidual immune cells, comprising about one-third of all maternal decidual cells and two-thirds of decidual immune cells. dNK cells are replaced by decidual CD8$^+$ T cells as pregnancy advances (Paffaro et al., 2003). Although depletion of NK cells, but not CD8$^+$ cells, increased bacterial loads in the spleen, liver, placenta, and fetus after 3 days of infection (before antigen-specific CD8$^+$ T cells have expanded), depletion of NK or CD8$^+$ T cells led to *Lm*-induced abortion in *GNLY*-Tg animals. Thus, NK and CD8$^+$ T cells contribute to fetal protection. CD8$^+$ T cell protection in pregnancy may be due to *Lm*-specific CD8$^+$ T cell control of systemic bacterial infection plus antimicrobial function in the decidua nearer to term. In line with this, neither *Prf1*$^{-/-}$ WT nor *Prf1*$^{-/-}$ *GNLY*-Tg mice gave birth to viable pups when challenged with sublethal *Lm* (data not shown). Bacterial loads in *Prf1*$^{-/-}$ *GNLY*-Tg mice, however, were reduced significantly compared with *Prf1*$^{-/-}$ mice lacking the transgene both systemically and in the fetus (data not shown). The difference in pregnancy outcome between PFN-deficient and -sufficient mice suggests that granule (and PFN)-dependent and -independent mechanisms contribute to *Lm* protection in pregnancy. GNLY and PFN are likely important in CD8$^+$ T cell control of systemic infection by killing infected host cells and suppressing bacteria within them, as demonstrated previously in nonpregnant mice (Walch et al., 2014). PFN-dependent protection by degranulation of peripheral (and possibly decidual) CD8 T cells later in pregnancy likely explains why no *Prf1*$^{-/-}$ mice had successful pregnancies even when they expressed GNLY. At present, there are no ways to assess the importance of GNLY or PFN in dNK versus pNK cells by conditionally expressing or knocking out genes only in decidual lymphocytes.

GNLY transfer from dNK to JEG-3 cells and EVTs was actin dependent via nanotubes, which also transferred CFSE and DiO, but not GzmB, unidirectionally from dNK to target cells. GNLY transfer occurred rapidly within minutes of co-culture

and was incredibly efficient because co-cultured trophoblasts stained almost as brightly for GNLY as dNK cells. Nanotube formation and GNLY transfer were constitutive and did not change with target cell infection. The presence of GNLY in uninfected cells could prevent bacterial replication as soon as cells became infected. In other systems, nanotube transport of small cytosolic molecules depends on the actin cytoskeleton, whereas transport of organelles depends on microtubules (Kimura et al., 2012). Here, the nanotube connections between NK and JEG-3 cells stained for actin but infrequently for tubulin. GNLY transfer and *Lm* killing were inhibited by blocking actin polymerization but not by inhibiting endocytosis or microtubules. Nocodazole inhibited GNLY transfer in the first 15 min, but after 3 h of NK:JEG-3 cell coincubation in the presence of nocodazole, enough GNLY was transferred to kill intracellular bacteria. This initial difference may indicate that microtubules are involved in initiating nanotubes or in GNLY trafficking to the nanotube. Indeed, the SIM images (Figure 5) suggest that GNLY accumulates near the origin of the nanotube. Nanotube formation likely requires receptor-ligand interactions between the connecting cells, but blocking cell-surface receptors that mediate dNK cell-EVT interactions did not interfere with nanotube connections or GNLY transfer. Neuraminidase treatment of the target inhibited GNLY transfer, suggesting that binding of dNK cell receptor(s) to sialylated protein(s) on the target cell promotes nanotube formation. The lack of inhibition by single blocking antibodies could be due to redundancy of receptors that mediate nanotube formation. Further work is needed to understand how nanotube connections are formed.

In addition to direct transfer to target cells, dNK cells secrete GNLY into culture supernatants (Figures 1B and 1C), which kills extracellular *Lm* but not *Lm* in trophoblasts (Figure 2A). These results suggest that dNK cell secretion of GNLY might help control cell-free bacteria before they invade trophoblasts and also control infection by bacteria whose lifestyle is primarily extracellular. However, even a 1:1 dilution of dNK cell culture supernatants (data not shown) or pNK cell culture supernatants was inactive against extracellular *Lm*. Intracellular *L. innocua* have been shown previously to be killed in DCs by micromolar concentrations of recombinant GNLY in the culture medium (Walch et al., 2005). Based on the level of secreted GNLY in the culture medium (<10 nM), secreted GNLY may not reach the *in vivo* concentrations needed to kill extracellular bacteria. Although the concentration of secreted GNLY in uterine, decidual, and placental fluids is unknown and will be difficult to measure, *GNLY*-Tg mice could be used to study the role of secreted GNLY in controlling infection with extracellular pathogens, such as GBS.

Decidual and pNK cells selectively killed an intracellular microbe without destroying the host cell. The key to selective bacterial killing is selective transfer of GNLY but not cytotoxic granules or other cytotoxic granule components that would kill the host cell. Although we showed that small dyes were also transferred from dNK cells to trophoblasts, we did not examine whether additional endogenous proteins were also transferred or whether nanotube connections altered the properties or functions of the connected cell. Although crosstalk between dNK cells and EVTs to facilitate placentation has been assumed to be mediated by uptake of dNK cell-secreted growth factors and cytokines, direct transfer of cytosolic proteins and other molecules, including nutrients, by nanotubes could contribute to dNK regulation of placentation.

dNK cells are not the only killer cells to transfer GNLY to selectively kill intracellular bacteria, and trophoblasts are not the only target cell in which *Lm* could be suppressed without killing the host cell. pNK cells also transfer GNLY, form nanotube connections, and selectively kill bacteria in trophoblasts, macrophages and DCs. Although nanotube connections by pNK and T cells have been observed previously (Chauveau et al., 2010; Davis and Sowinski, 2008; Önfelt et al., 2004; Sowinski et al., 2008), their function was not clear. dNK cells express much more GNLY than pNK cells, whereas GNLY transfer from pNK cells was only detected when GNLY levels were increased by cytokine activation. Nonetheless, even though GNLY transfer by freshly isolated pNK cells was below the level of detection, pNK cells had anti-bacterial potency comparable with dNK cells in multiple experiments (Figures 2B–2E, 3A, 4H, 6F, S5C, and S5G). These results suggest that dNK cells have a surfeit of GNLY, much more than what is needed to kill intracellular bacteria. pNK cell killing, despite low levels of GNLY, recalls the potent cytolytic activity of PFN, which can kill target cells even when it is below the detection limit of flow cytometry (Nagler-Anderson et al., 1989). It is worth investigating whether GNLY-expressing adaptive and innate-like cytotoxic T cells also use nanotubes to selectively transfer GNLY for anti-microbial defense. This immune defense may be important in immune-privileged sites, where killer lymphocyte-mediated degranulation is suppressed, or against infected target cells that are resistant to conventional granule-mediated cytotoxicity. Although GNLY was efficiently transferred by dNK and pNK cells to other cell types, bacteria were only killed in EVTs, macrophages, and DCs but not in HeLa, HFFs, or a glioblastoma cell line. What distinguishes cells in which bacteria are killed is not clear, except that GNLY localized more with bacteria in those cells. All cells in which bacteria were killed (including EVTs) are highly phagocytic, which might affect trafficking of bacteria or GNLY.

This study demonstrates an unexpected role of dNK cells in providing immunity to placental infection. The constraints of maternal-fetal tolerance, which interferes with unleashing the full power of cytotoxic granules to fight infection, lead to more serious infection during pregnancy. Although GNLY transfer via nanotubes may not be as powerful as degranulation for controlling intracellular microbes, our *in vivo* comparison of *Lm* infection in WT and *GNLY*-Tg mice indicates a profound GNLY-dependent improvement in pregnancy outcome after *Lm* infection. Further understanding the molecular mechanisms responsible for GNLY transfer and intracellular bacterial killing may provide insights into how mother-to-fetus transmission of infection could be treated better.

STAR★METHODS

Detailed methods are provided in the online version of this paper and include the following:

- KEY RESOURCE TABLE

SUPPLEMENTAL INFORMATION

Supplemental Information can be found online at https://doi.org/10.1016/j.cell.2020.07.019.

ACKNOWLEDGMENTS

We thank Harry Leung (PCMM Microscopy Core) for help with live imaging, Strominger lab members for help with processing placental tissues, and Ana Gadish-Linares for designing the graphical abstract. This work was supported by NIH (United States) grants HD87689 and AI45862 (to J.L.S. and J.L.).

AUTHOR CONTRIBUTIONS

A.C.C., S.M., and F.D. designed and performed experiments, analyzed the data, and assisted with writing the manuscript. J.A.A., K.I., C.O., S.S.S. and C.J. performed experiments. J.L. conceived the study. J.L., T.T., and J.L.S. designed the experimental plan, interpreted data, and wrote the manuscript.

DECLARATION OF INTERESTS

The authors declare no competing interests.

Received: February 4, 2020
Revised: May 26, 2020
Accepted: July 14, 2020
Published: August 20, 2020

REFERENCES

Apps, R., Murphy, S.P., Fernando, R., Gardner, L., Ahad, T., and Moffett, A. (2009). Human leucocyte antigen (HLA) expression of primary trophoblast cells and placental cell lines, determined using single antigen beads to characterize allotype specificities of anti-HLA antibodies. Immunology *127*, 26–39.

Berges, C., Naujokat, C., Tinapp, S., Wieczorek, H., Höh, A., Sadeghi, M., Opelz, G., and Daniel, V. (2005). A cell line model for the differentiation of human dendritic cells. Biochem. Biophys. Res. Commun. *333*, 896–907.

Błaszkowska, J., and Góralska, K. (2014). Parasites and fungi as a threat for prenatal and postnatal human development. Ann. Parasitol. *60*, 225–234.

Cao, B., and Mysorekar, I.U. (2014). Intracellular bacteria in placental basal plate localize to extravillous trophoblasts. Placenta *35*, 139–142.

Chauveau, A., Aucher, A., Eissmann, P., Vivier, E., and Davis, D.M. (2010). Membrane nanotubes facilitate long-distance interactions between natural killer cells and target cells. Proc. Natl. Acad. Sci. USA *107*, 5545–5550.

Crespo, Â.C., Strominger, J.L., and Tilburgs, T. (2016). Expression of KIR2DS1 by decidual natural killer cells increases their ability to control placental HCMV infection. Proc. Natl. Acad. Sci. USA *113*, 15072–15077.

Crespo, Â.C., van der Zwan, A., Ramalho-Santos, J., Strominger, J.L., and Tilburgs, T. (2017). Cytotoxic potential of decidual NK cells and CD8+ T cells awakened by infections. J. Reprod. Immunol. *119*, 85–90.

Crocker, P.R., Paulson, J.C., and Varki, A. (2007). Siglecs and their roles in the immune system. Nat. Rev. Immunol. *7*, 255–266.

Davis, D.M., and Sowinski, S. (2008). Membrane nanotubes: dynamic long-distance connections between animal cells. Nat. Rev. Mol. Cell Biol. *9*, 431–436.

Dotiwala, F., and Lieberman, J. (2019). Granulysin: killer lymphocyte safeguard against microbes. Curr. Opin. Immunol. *60*, 19–29.

Dotiwala, F., Mulik, S., Polidoro, R.B., Ansara, J.A., Burleigh, B.A., Walch, M., Gazzinelli, R.T., and Lieberman, J. (2016). Killer lymphocytes use granulysin, perforin and granzymes to kill intracellular parasites. Nat. Med. *22*, 210–216.

Dotiwala, F., Sen Santara, S., Binker-Cosen, A.A., Li, B., Chandrasekaran, S., and Lieberman, J. (2017). Granzyme B Disrupts Central Metabolism and Protein Synthesis in Bacteria to Promote an Immune Cell Death Program. Cell *171*, 1125–1137.e11.

Erlebacher, A. (2013). Immunology of the maternal-fetal interface. Annu. Rev. Immunol. *31*, 387–411.

Hanna, J., Goldman-Wohl, D., Hamani, Y., Avraham, I., Greenfield, C., Natanson-Yaron, S., Prus, D., Cohen-Daniel, L., Arnon, T.I., Manaster, I., et al. (2006). Decidual NK cells regulate key developmental processes at the human fetal-maternal interface. Nat. Med. *12*, 1065–1074.

Huang, L.P., Lyu, S.C., Clayberger, C., and Krensky, A.M. (2007). Granulysin-mediated tumor rejection in transgenic mice. J. Immunol. *178*, 77–84.

Kimura, S., Hase, K., and Ohno, H. (2012). Tunneling nanotubes: emerging view of their molecular components and formation mechanisms. Exp. Cell Res. *318*, 1699–1706.

King, A., Wooding, P., Gardner, L., and Loke, Y.W. (1993). Expression of perforin, granzyme A and TIA-1 by human uterine CD56+ NK cells implies they are activated and capable of effector functions. Hum. Reprod. *8*, 2061–2067.

Koopman, L.A., Kopcow, H.D., Rybalov, B., Boyson, J.E., Orange, J.S., Schatz, F., Masch, R., Lockwood, C.J., Schachter, A.D., Park, P.J., and Strominger, J.L. (2003). Human decidual natural killer cells are a unique NK cell subset with immunomodulatory potential. J. Exp. Med. *198*, 1201–1212.

Kopcow, H.D., Allan, D.S.J., Chen, X., Rybalov, B., Andzelm, M.M., Ge, B., and Strominger, J.L. (2005). Human decidual NK cells form immature activating synapses and are not cytotoxic. Proc. Natl. Acad. Sci. USA *102*, 15563–15568.

Manaster, I., and Mandelboim, O. (2010). The unique properties of uterine NK cells. Am. J. Reprod. Immunol. *63*, 434–444.

Moffett-King, A. (2002). Natural killer cells and pregnancy. Nat. Rev. Immunol. *2*, 656–663.

Nagler-Anderson, C., Lichtenheld, M., Eisen, H.N., and Podack, E.R. (1989). Perforin mRNA in primary peritoneal exudate cytotoxic T lymphocytes. J. Immunol. *143*, 3440–3443.

Önfelt, B., Nedvetzki, S., Yanagi, K., and Davis, D.M. (2004). Cutting edge: Membrane nanotubes connect immune cells. J. Immunol. *173*, 1511–1513.

Paffaro, V.A., Jr., Bizinotto, M.C., Joazeiro, P.P., and Yamada, A.T. (2003). Subset classification of mouse uterine natural killer cells by DBA lectin reactivity. Placenta *24*, 479–488.

Rasmussen, C.A., Pace, J.L., Banerjee, S., Phillips, T.A., and Hunt, J.S. (1999). Trophoblastic cell lines generated from tumour necrosis factor receptor-deficient mice reveal specific functions for the two tumour necrosis factor receptors. Placenta *20*, 213–222.

Rizzuto, G.A., Kapidzic, M., Gormley, M., and Bakardjiev, A.I. (2016). Human Placental and Decidual Organ Cultures to Study Infections at the Maternal-fetal Interface. J. Vis. Exp. *113*, e54237.

Robbins, J.R., Skrzypczynska, K.M., Zeldovich, V.B., Kapidzic, M., and Bakardjiev, A.I. (2010). Placental syncytiotrophoblast constitutes a major barrier to vertical transmission of Listeria monocytogenes. PLoS Pathog. *6*, e1000732.

Schneider, C.A., Rasband, W.S., and Eliceiri, K.W. (2012). NIH Image to ImageJ: 25 years of image analysis. Nat. Methods *9*, 671–675.

Siewiera, J., El Costa, H., Tabiasco, J., Berrebi, A., Cartron, G., Le Bouteiller, P., and Jabrane-Ferrat, N. (2013). Human cytomegalovirus infection elicits new decidual natural killer cell effector functions. PLoS Pathog. *9*, e1003257.

Sowinski, S., Jolly, C., Berninghausen, O., Purbhoo, M.A., Chauveau, A., Köhler, K., Oddos, S., Eissmann, P., Brodsky, F.M., Hopkins, C., et al. (2008). Membrane nanotubes physically connect T cells over long distances presenting a novel route for HIV-1 transmission. Nat. Cell Biol. *10*, 211–219.

Stenger, S., Hanson, D.A., Teitelbaum, R., Dewan, P., Niazi, K.R., Froelich, C.J., Ganz, T., Thoma-Uszynski, S., Melián, A., Bogdan, C., et al. (1998). An antimicrobial activity of cytolytic T cells mediated by granulysin. Science *282*, 121–125.

Thiery, J., Walch, M., Jensen, D.K., Martinvalet, D., and Lieberman, J. (2010). Isolation of cytotoxic T cell and NK granules and purification of their effector proteins. Curr. Protoc. Cell Biol. *Chaper 3*, Unit 3.37.

Tilburgs, T., Evans, J.H., Crespo, Â.C., and Strominger, J.L. (2015a). The HLA-G cycle provides for both NK tolerance and immunity at the maternal-fetal interface. Proc. Natl. Acad. Sci. USA *112*, 13312–13317.

Tilburgs, T., Crespo, Â.C., van der Zwan, A., Rybalov, B., Raj, T., Stranger, B., Gardner, L., Moffett, A., and Strominger, J.L. (2015b). Human HLA-G+ extravillous trophoblasts: Immune-activating cells that interact with decidual leukocytes. Proc. Natl. Acad. Sci. USA *112*, 7219–7224.

Vujaklija, D.V., Gulic, T., Sucic, S., Nagata, K., Ogawa, K., Laskarin, G., Saito, S., Haller, H., and Rukavina, D. (2011). First trimester pregnancy decidual natural killer cells contain and spontaneously release high quantities of granulysin. Am. J. Reprod. Immunol. *66*, 363–372.

Walch, M., Eppler, E., Dumrese, C., Barman, H., Groscurth, P., and Ziegler, U. (2005). Uptake of granulysin via lipid rafts leads to lysis of intracellular Listeria innocua. J. Immunol. *174*, 4220–4227.

Walch, M., Dotiwala, F., Mulik, S., Thiery, J., Kirchhausen, T., Clayberger, C., Krensky, A.M., Martinvalet, D., and Lieberman, J. (2014). Cytotoxic cells kill intracellular bacteria through granulysin-mediated delivery of granzymes. Cell *157*, 1309–1323.

Zeldovich, V.B., and Bakardjiev, A.I. (2012). Host defense and tolerance: unique challenges in the placenta. PLoS Pathog. *8*, e1002804.

Zhang, J., Dong, Z., Zhou, R., Luo, D., Wei, H., and Tian, Z. (2005). Isolation of lymphocytes and their innate immune characterizations from liver, intestine, lung and uterus. Cell. Mol. Immunol. *2*, 271–280.

Zheng, C.F., Ma, L.L., Jones, G.J., Gill, M.J., Krensky, A.M., Kubes, P., and Mody, C.H. (2007). Cytotoxic CD4+ T cells use granulysin to kill Cryptococcus neoformans, and activation of this pathway is defective in HIV patients. Blood *109*, 2049–2057.

STAR★METHODS

KEY RESOURCE TABLE

REAGENT or RESOURCE	SOURCE	IDENTIFIER
Antibodies		
Pacific Orange mouse anti-human CD45	ThermoFisher Scientific	Clone HI30; Cat.# MHCD4530; RRID:AB_10376143
APC mouse anti-human CD45	BioLegend	Clone HI30; Cat.# 304012; RRID:AB_314400
Purified mouse anti-human CD45	BioLegend	Clone HI30; Cat.# 304002; RRID: AB_314390
PE mouse anti-human CD56	BioLegend	Clone HCD56; Cat.# 318306; RRID:AB_604101
AlexaFluor 700™ mouse anti-human CD56	BioLegend	Clone HCD56; Cat.# 318316; RRID:AB_604104
AlexaFluor 647™ mouse anti-human CD56	BioLegend	Clone HCD56; Cat.# 318314; RRID:AB_604103
Pacific Blue mouse anti-human CD56	BioLegend	Clone HCD56; Cat.# 318326; RRID:AB_10612751
Pacific Blue mouse anti-human CD14	BioLegend	Clone HCD14; Cat.# 325616; RRID:AB_830689
AlexaFluor 647™ mouse anti-human CD14	BioLegend	Clone HCD14; Cat.# 325612; RRID:AB_830685
PE-Cy7 mouse anti-human CD14	BioLegend	Clone M5E2; Cat.# 301814; RRID:AB_389353
AlexaFluor 700™ mouse anti-human CD8	BioLegend	Clone SK1; Cat.# 344724; RRID:AB_2562790
PerCP mouse anti-human CD8	BioLegend	Clone SK1; Cat.# 344708; RRID:AB_1967149
PE mouse anti-human CD8	BioLegend	Clone SK1; Cat.# 344706; RRID:AB_1953244
PE mouse anti-human HLA-G	Abcam	Clone MEM-G/9; Cat.# ab24384; RRID:AB_448029
APC mouse anti-human HLA-G	ThermoFisher Scientific	Clone MEM-G/9; Cat.# A15708; RRID:AB_2534488
Purified mouse anti-human HLA-G	Abcam	Clone 4H84; Cat.# ab52455; RRID:AB_880552
Purified mouse anti-human HLA-G	BioLegend	Clone 87G; Cat.# 335904; RRID: AB_10641840
AlexaFluor 488™ mouse anti-human Granzyme A	BioLegend	Clone CB9; Cat.# 507212; RRID:AB_528909
PE-Texas Red mouse anti-human Granzyme B	ThermoFisher Scientific	Clone GB11; Cat.# GRB17; RRID:AB_2536540
AlexaFluor 647™ mouse anti-human Granzyme B	BioLegend	Clone GB11; Cat.# 515406; RRID:AB_2566333
AlexaFluor 647™ mouse anti-human Perforin	BioLegend	Clone dG9; Cat.# 308110; RRID:AB_493254
Pacific Blue mouse anti-human Perforin	BioLegend	Clone dG9; Cat.# 308118; RRID:AB_10899565
Purified mouse anti-human Perforin	BioLegend	Clone dG9; Cat.# 308102; RRID:AB_314700
PE mouse anti-human Granulysin	BioLegend	Clone DH2; Cat.# 348004; RRID:AB_2263307
AlexaFluor 647™ mouse anti-human Granulysin	BioLegend	Clone DH2; Cat.# 348006; RRID:AB_2110110
AlexaFluor 488™ mouse anti-human Granulysin	BD Biosciences	Clone RB1; Cat.# 558254
Purified mouse anti-human Granulysin	MBL International	Clone RF10; Cat.# D186-3; RRID:AB_591809
AlexaFluor 647™ mouse anti-human CD11a (LFA-1)	BioLegend	Clone HI111; Cat.# 301218; RRID:AB_2128991
Purified mouse anti-human CD11a (LFA-1)	BioLegend	Clone HI111; Cat.# 301202; RRID:AB_314140
Pacific Blue rat anti-human CD49f	BioLegend	Clone GoH3; Cat.# 313620; RRID:AB_2128018
Purified rat anti-human CD49f	BioLegend	Clone GoH3; Cat.# 313602; RRID:AB_345296
Purified goat anti-human B7-H3	R&D Systems	Polyclonal; Cat.# AF1027; RRID:AB_354546
Purified rabbit anti-human α-tubulin	Cell Signaling	Polyclonal; Cat.# 2148S; RRID:AB_2288042
PE-Cy7 mouse anti-human B7-H3	BioLegend	Clone MIH42; Cat.# 351008; RRID:AB_2564555
PerCP-Cy5.5 mouse anti-human CD107a	BioLegend	Clone H4A3; Cat.# 328616; RRID:AB_1227508
Purified mouse anti-human E-Cadherin (CDH-1)	GeneTex	Clone G-4770; Cat.# GTX100443S; RRID:AB_10720531
Purified rat anti-human E-cadherin (CD324)	eBioscience	Clone: DECMA-1; Cat.# 16-3249-82; RRID: AB_10734213
PE-Cy7 mouse anti-human E-Cadherin	BioLegend	Clone: 67A4; Cat.# 324115; RRID: AB_2563095

(*Continued on next page*)

Continued

REAGENT or RESOURCE	SOURCE	IDENTIFIER
Purified rabbit anti-*Listeria monocytogenes*	Abcam	Polyclonal; Cat.# ab35132; RRID:AB_776048
Purified mouse anti-human CD104	BioLegend	Clone 58XB4; Cat.# 327802; RRID: AB_893212
Purified mouse anti-human CD58 (LFA-3)	BioLegend	Clone TS2/9; Cat.# 330911; RRID: AB_2291391
APC mouse anti-human CD58	BioLegend	Clone TS2/9; Cat.# 330917; RRID: AB_2650885
Purified mouse anti-human CD2	BioLegend	Clone RPA-2.10; Cat.# 300212; RRID: AB_314036
FITC mouse anti-human CD2	BioLegend	Clone RPA-2.10; Cat.# 300206; RRID: AB_314030
PE mouse anti-human NKG2A	Beckman Coulter	Clone Z199; Cat.# IM3291U; RRID: AB_10643228
Purified mouse anti-human KIR2DL1/S1/S3/S5	BioLegend	Clone HP-MA4; Cat.# 339502; RRID: AB_1501078
Purified mouse anti-human KIR2DL2/L3/S2	BioLegend	Clone DX27; Cat.# 312602; RRID: AB_314933
Purified mouse anti-human KIR2DL4	BioLegend	Clone mAb 33; Cat.# 347003; RRID: AB_2028425
Purified mouse anti-human ILT-2 (LILRB1)	BioLegend	Clone GHI/75; Cat.# 333704; RRID:AB_1089088
Purified mouse anti-human HLA-A, B, C	BioLegend	Clone W6/32; Cat.# 311428; RRID: AB_2561492
Purified mouse anti-human CD43	Invitrogen	Clone: MEM-59; Cat.# MA-1-19009; RRID: AB_1072361
FITC mouse anti-human CD43	BioLegend	Clone MEM-59; Cat.# 315203; RRID: AB_389246
AlexaFluor 647™ mouse anti-human Siglec-7	R&D Systems	Clone 194211; Cat.# FAB11381R-100UG;
Purified goat anti-human Siglec-7	Invitrogen	Polyclonal; Cat.# PA5-47079; RRID: AB_2576436
Mouse IgG1	BioLegend	Clone MOPC-21; Cat.# 400102;
Mouse IgG2a	BioLegend	Clone MOPC-173; Cat.# 400202
Mouse IgG2b	BioLegend	Clone 27-35; Cat.# 402202
Normal goat IgG	R&D Systems	Polyclonal; Cat.# AB-108-C
AlexaFluor 488™ mouse IgG1 Isotype control	BioLegend	Clone MOPC-21; Cat.# 400129
PE mouse IgG1 Isotype control	BioLegend	Clone MOPC-21; Cat.# 400113; RRID:AB_326435
AlexaFluor 647™ mouse IgG1 Isotype control	BioLegend	Clone MOPC-21; Cat.# 400130;
PerCP-Cy5.5 mouse IgG1 Isotype control	BioLegend	Clone MOPC-21; Cat.#400150; RRID:AB_893664
AlexaFluor 488™ mouse IgG2a Isotype control	BioLegend	Clone MOPC-173; Cat.# 400233;
AlexaFluor 647™ mouse IgG2b Isotype control	BioLegend	Clone MPC-11; Cat.# 400330;
Pacific Blue mouse IgG2b isotype control	BioLegend	Clone MPC-11; Cat.# 400331
PerCP-Cy5.5 hamster anti-mouse CD3	BD Biosciences	Clone 145-2C11; Cat.# 100328; RRID: AB_893318
APC rat anti-mouse CD8α	BioLegend	Clone 53-6.7; Cat.# 100712; RRID: AB_312751
PE rat anti-mouse CD45	BD Biosciences	Clone 30-F11; Cat.# 553081; RRID: AB_394611
FITC rat anti-mouse NKp46	BioLegend	Clone 29A1.4; Cat.# 137606; RRID: AB_2298210
PE-Cy7 rat anti-mouse CD4	BioLegend	Clone GK1.5; Cat.# 100422; RRID: AB_312707
Donkey anti-Goat IgG (H+L) Cross-Adsorbed Secondary Antibody, Alexa Fluor 568™	Thermofisher Scientific	Polyclonal; Cat.# A-11057; RRID:AB_2534104
Donkey anti-Mouse IgG (H+L) Highly Cross-Adsorbed Secondary Antibody, Alexa Fluor 647™	Thermofisher Scientific	Polyclonal; Cat.# A-31571; RRID:AB_162542
Goat anti-Rat IgG (H+L) Cross-Adsorbed Secondary Antibody, Cyanine3	Thermofisher Scientific	Polyclonal; Cat.# A10522; RRID:AB_2534031
Donkey anti-Rabbit IgG (H+L) Highly Cross-Adsorbed Secondary Antibody, Alexa Fluor Plus 488™	Thermofisher Scientific	Polyclonal; Cat.# A32790; RRID:AB_2762833
Biotin mouse anti-human Granulysin	BioLegend	Clone DH10; Cat.# 526104; RRID:AB_2563604
Purified goat anti-human Granulysin	R&D Systems	Polyclonal; Cat.# AF3138 RRID: AB_2232321
Purified mouse anti-human β-actin	Iowa University DSHB	Cat.# JLA20; RRID:AB_528068
Purified rat anti–mouse CD4	BioXCell	Clone GK 1.5; Cat.# BE0003-1; RRID:AB_1107636
Purified rat anti–mouse CD8α	BioXCell	Clone 2.43; Cat.# BE0061; RRID:AB_1125541
Purified rabbit anti–mouse asialo-GM1	Wako Chemicals	Antiserum; Cat.# 986-10001; RRID:AB_516844
Purified rat IgG2b Isotype control	BioXCell	Clone LTF-2; Cat.# BE0090; RRID:AB_1107780

(*Continued on next page*)

Continued

REAGENT or RESOURCE	SOURCE	IDENTIFIER
Bacterial and Virus Strains		
Listeria monocytogenes (10403)	Lab strain	N/A
Biological Samples		
Human decidual and placental tissue (from 6-12 week gestation elective terminations)	Local reproductive health clinic	N/A
Healthy donor PBMC from blood donations	Brigham and Women's Hospital	https://researchcores.partners.org/crim/about;
Chemicals, Peptides, and Recombinant Proteins		
DPBS	GIBCO	Cat.# 14190250
HBSS	Corning	Cat.# 21-022-CV
DMEM	GIBCO	Cat.# 11965092
RPMI 1640	Corning	Cat. # 15-040-CV
DMEM/F12	GIBCO	Cat.# 11320033
Newborn Calf Serum	GIBCO	Cat.# 16010159
Fetal Calf Serum	X&Y Cell Culture	Cat.# FBS-500-HI
Penicillin/Streptomycin	GIBCO	Cat.# 15140122
L-glutamine	GIBCO	Cat.# 25030081
TrypLE Express	ThermoFisher Scientific	Cat.# 12605036
Trypsin from porcine pancreas lyophilized powder, Type II-S	Sigma	Cat.# T7409-100G; CAS: 9002-07-7
EDTA, disodium, dihydrate	American Bioanalytical	Cat.# AB00500-00100; CAS: 6381-92-6
Ficoll® Paque Plus	GE Healthcare	Cat.# GE17-1440-02
Human Fibronectin	Corning	Cat.# 354008; GenPept: P02751.5
Collagenase type IV from *Clostridium histolyticum*	Sigma	Cat.# C5138-5G; CAS: 9001-12-1
Collagenase D from *Clostridium histolyticum*	Roche	Cat.# 11088882001; CAS: 9001-12-1
Deoxyribonuclease I from bovine pancreas	Sigma	Cat.# DN25-G5; CAS: 9003-98-9
Deoxyribonuclease I from bovine pancreas	Roche	Cat.# 11284932001; CAS: 9003-98-9
Red Blood Cell Lysing Buffer Hybri-Max™	Sigma	Cat.# R7757-100ML
Percoll	GE Healthcare	Cat.# 17089109
Matrigel	Corning	Cat.# 354234
Gentamicin	GIBCO	Cat.# 15750060
Amphotericin B	Sigma	Cat.# A2942-20ML CAS: 1397-89-3
X-Vivo 10 Serum free hematopoietic cell medium (without gentamicin or phenol red)	Lonza	Cat.# 04-743Q
Human AB Serum	Corning (Fisher Scientific)	Cat.# MT-35-060-CI
Recombinant human IL-15	BioLegend	Cat.# 715902; GenPept: P40933.1
Recombinant mouse IL-15	R&D	Cat.# 447-ML-010; GenPept: P48346.1
Recombinant human IL-2	R&D	Cat.# GenPept: P60568.1
Recombinant human IL-4	R&D Technologies	Cat.# 204-IL-050; GenPept: P05112.1
Recombinant human GM-CSF	R&D Technologies	Cat.# 215-GM-50; GenPept: P04141.1
Recombinant human TNF-α	eBioscience	Cat .# 14-8329-63; GenPept: P01375.1
Ionomycin calcium salt	Sigma	Cat.# I0634-1MG; CAS: 56092-82-1
Insulin-Transferrin-Selenium (ITS-G)	GIBCO	Cat.# 41400045
Recombinant human EGF	Peprotech	Cat.# AF-100-15; GenPept: P01133.2
Human chorionic gonadotropin	Sigma	Cat.# C1063-1VL; CAS: 9002-61-3
Bacto Brain Heart Infusion	BD Biosciences	Cat.# 237500
Agar	Criterion	Cat.# CS5002; CAS: 9002-18-0
Streptomycin sulfate	Sigma	Cat.# 1623003; CAS: 3810-74-0

(*Continued on next page*)

Continued

REAGENT or RESOURCE	SOURCE	IDENTIFIER
GNLY purified from YT-Indy cytotoxic granules	Lieberman Lab	Thiery et al., 2010
RIPA buffer	Sigma	Cat.# R0278-50ML; MDL: MFCD02100484
NuPAGE LDS Sample Buffer (4X)	ThermoFisher Scientific	Cat.# NP0007
β-Mercaptoethanol, Molecular Biology Grade	Sigma	Cat.# 444203; CAS: 60-24-2
Chromium-51 Radionuclide	Perkin Elmer	Cat.# NEZ030001MC; CAS: 16284-59-6
Protein Transport Inhibitor (Containing Brefeldin A)	BD Biosciences	Cat.# 555029
EGTA	Sigma	Cat.# E3889-100G CAS: 67-42-5
Cytochalasin D	Sigma	Cat.# C8273; CAS: 22144-77-0
Dynasore	Sigma	Cat. 324410 CAS: 304448-55-3
3,4-Dichloroisocoumarin (DCI)	Sigma	Cat.# D7910; CAS: 51050-59-0
α2′3,6,8,9 neuraminidase	New England Biolabs	Cat.# P0722S
Nocodazole	Sigma	Cat.# M1404-10MG; CAS: 31430-18-9
Poly-L-lysine solution	Sigma	Cat.# P8920; CAS: P8920-100ML
Formaldehyde, 16%, methanol free, Ultra Pure	Polysciences, Inc	Cat.# 18814-10; CAS: 50-00-0
BSA	Sigma	Cat.# A9418-500G CAS: 9048-46-8
Triton X-100	Sigma	Cat.# X100-500ML; CAS: 9002-93-1
Hoechst 33342	Immunochemistry Technologies	Cat.# 639
DAPI	Thermo Scientific	Cat.# 62248
Rhodamine Phalloidin	ThermoFisher Scientific	Cat.# R415
Airvol ® 205 Polyvinyl alcohol	Air Products and Chemicals	N/A
Sucrose	Sigma	Cat.# S8501 CAS: 57-50-1
O.C.T. Compound	Tissue Tek	Cat.# 4583
Glycine	Sigma	Cat.# 50046; CAS: 7299-33-4
Tween 20	Sigma	Cat.# P1379-500ML CAS: 9005-64-5
Critical Commercial Assays		
RosetteSep Human NK Cell Enrichment Cocktail	STEMCELL Technologies	Cat.# 15065
NK Cell Isolation Kit, mouse	Miltenyi Biotec	Cat.# 130-115-818
Human BD Fc Block	BD Biosciences	Cat.# 564219
Fixation/Permeabilization Solution Kit	BD Biosciences	Cat.# 554714
LEGEND MAX Human Granulysin ELISA Kit	BioLegend	Cat.# 438007
MILLIPLEX MAP Human CD8+ T Cell Magnetic Bead Panel	Millipore	Cat.# HCD8MAG-15K
Dynabeads Protein G Immunoprecipitation Kit	ThermoFisher Scientific	Cat. # 10007D
cOmplete Protease Inhibitor Cocktail	Roche	Cat.# 11697498001
Mitotracker Deep Red FM	ThermoFisher Scientific	Cat.# M22426
DNeasy Blood and Tissue Kit	QIAGEN	Cat.# 69504
Zombie Yellow Fixable Viability Kit	BioLegend	Cat.# 423104
CellTrace Far Red DDAO-SE. Kit	ThermoFisher Scientific	Cat.# C34564
CellTracker Deep Red Dye	ThermoFisher Scientific	Cat.# C34565
Vybrant DiO Cell-Labeling Solution	ThermoFisher Scientific	Cat.# V22886
CFSE Cell Division Tracker Kit	BioLegend	Cat.# 423801
Mix-n-Stain CF405 Dye Antibody Labeling Kit	Biotium	Cat.# 92305
Mix-n-Stain CF488 Dye Antibody Labeling Kit	Biotium	Cat.# 92233
Mix-n-Stain CF568 Dye Antibody Labeling Kit	Biotium	Cat.# 92235
Mix-n-Stain CF647 Dye Antibody Labeling Kit	Biotium	Cat.# 92238
Experimental Models: Cell Lines		
JEG-3		N/A
LCL 721.221	ATCC	Cat.# CRL-1855RRID: CVCL_6263

(*Continued on next page*)

Continued

REAGENT or RESOURCE	SOURCE	IDENTIFIER
HeLa	ATCC	Cat.#: CRM-CCL-2; RRID:CVCL_0030
HFF	ATCC	Cat.#: SCRC-1041; RRID:CVCL_3285
YAC-1	ATCC	Cat.#: TIB-160; RRID:CVCL_2244
U-251	A. Krichevsky (BWH)	RRID:CVCL_0021
THP-1	ATCC	Cat.#: TIB-202; RRID:CVCL_0006
SM9-1	M. Petroff (MSU)	N/A
YT-Indy	Z. Brahmi (Indiana U.)	N/A
Experimental Models: Organisms/Strains		
Mouse: BALB/c		N/A
Mouse: *GNLY*-Tg BALB/c	Lieberman Lab	N/A
Mouse: *Prf1*$^{-/-}$ BALB/c	Jackson Labs, backcrossed in Lieberman Lab	N/A
Mouse: *GNLY*-Tg *Prf1*$^{-/-}$ BALB/c	Lieberman Lab	N/A
Software and Algorithms		
FlowJo V10	BD	https://www.flowjo.com/solutions/flowjo
INSPIRE and IDEAS	Luminex	https://www.luminexcorp.com/imaging-flow-cytometry/
SlideBook V5.0	Intelligent Imaging Innovations	https://www.intelligent-imaging.com/slidebook
ZEN Blue 2.0 and Lite	Zeiss	https://www.zeiss.com/microscopy/int/products/microscope-software/zen-lite.html
Prism 6.0	GraphPad	https://www.graphpad.com/scientific-software/prism/
ImageJ	Schneider et al., 2012	https://imagej.nih.gov/ij/
FV10-ASW version 03.00.01.15	Olympus	N/A

RESOURCE AVAILABILITY

Lead Contact

Further information and requests for resources and reagents should be directed and will be fulfilled by the Lead Contact, Judy Lieberman (judy.lieberman@childrens.harvard.edu)

Materials Availability

This study did not generate new unique reagents.

Data and Code Availability

This study did not generate datasets or code.

EXPERIMENTAL MODEL AND SUBJECT DETAILS

Human subjects

Human placental and decidual material were obtained from women undergoing elective pregnancy termination at a local clinic. All tissues were visually inspected for signs of excessive inflammation (including discoloration, large infarctions and foul odor) and only healthy tissues were used for further processing. Peripheral blood leukocytes were isolated from healthy volunteer blood donor leukopacks or collars. All human samples were de-identified, discarded clinical material and their use was approved by the Boston Children's Hospital and Harvard University human studies review boards. Placental and decidual sample gestational age ranged from 6 – 12 weeks. Human decidual samples were female, while the placental (fetal) sample sex and blood donor sex and age could not be determined due to constraints of the IRB protocol. The sample size for each experiment is given in the figure legend or shown in dot plots.

Cell lines

JEG-3 (male), 721.221 (female), YAC-1 (mouse lymphoma), YT-Indy (male) and SM9-1 (mouse trophoblast) were cultured in RPMI with 10% FCS supplemented with 1% Pen/Strep and 1% L-glutamine. HFF (male), U-251 (male) and HeLa (female) were cultured in DMEM with 10% FCS supplemented with 1% Pen/Strep and 1% L-glutamine. THP-1-derived DCs were obtained by culturing THP-1 in RPMI with 10% FCS, 1% Pen/Strep and 1% L-glutamine supplemented with 1500 IU/ml IL-4 and 1500 IU/ml GM-CSF changing the medium every 2 d. After 5 d, the medium was changed to serum-free RPMI supplemented with 3000 IU/ml IL-4, 1500 IU/ml GM-CSF, 2000 IU/ml TNF-α and 200 ng/ml ionomycin. Cells were cultured for 2 more d, and adherent cells were used (Berges et al., 2005). All cell lines were cultured at 37°C. Cell lines were recent passages and were periodically tested for mycoplasma contamination; flow cytometry was used to confirm surface markers. Whenever target cells were plated for bacterial infection, cells were washed three times in antibiotic-free medium immediately before infection or seeded for overnight culture in antibiotic-free media.

Mouse strains

GNLY-Tg C57BL/6, rederived at Jackson Laboratory as previously described (Huang et al., 2007; Walch et al., 2014), were backcrossed for more than 20 generations into the BALB/c background. These mice were crossed with *Prf1*$^{-/-}$ BALB/c mice (which were also generated by backcrossing *Prf1*$^{-/-}$ C57BL/6 (Jackson Laboratory) into the *BALB/c* background). All transgenic animals were bred and maintained in specific-pathogen free (SPF) conditions within the animal facility of Harvard Medical School until infection with *Listeria monocytogenes.* Virgin female mice (7-9 weeks old) were mated with male mice and the appearance of a vaginal plug was used to mark g.d. 0.5. Pregnant animals were infected on g.d. 6. All pregnant animals were included in the final analysis. Animal use was approved by the Animal Care and Use Committees of Boston Children's Hospital and Harvard Medical School.

Bacteria

L. monocytogenes (*Lm*) 10403S strain (Walch et al., 2014) was used. *Lm* were grown in 3.7% BHI with 50 μg/ml streptomycin at 37°C.

METHOD DETAILS

Experimental design

At least two biological replicates (donors) were performed for each experiment (human or mouse), except for immunoprecipitation of GNLY from dNK supernatants/lysates (Figure 1C), confocal microscopy imaging of isolated NK cells (Figures 1D and S1C), determination of GNLY and perforin/granzyme colocalization by imaging flow cytometry (Figures S1D and S1E), placental explant infection quantification by imaging (Figures 3B–3D), co-localization of GNLY with *Lm* in different cell targets (Figure S3) and LFA-1/granule polarization or nanotube quantification in NK:JEG-3 contacts under control conditions or after neuraminidase treatment (Figures S4B–S4E and S5E). None of the experiments were blinded. No statistical methods were used to predetermine sample size. Tissue from donors with a clinical history or symptoms of probable future miscarriage or infection, or tissue that was clearly inflamed or discolored were not used. No data were excluded from any of the experiments.

Isolation of NK cells, macrophages and trophoblasts

The procedure to isolate EVT, dNK and pNK was previously described (Tilburgs et al., 2015a). Briefly, decidual and villous tissues were macroscopically identified and separated. Primary cells were isolated from villous tissue by gently removing the basal membrane and digesting for 8 min at 37°C with 75 mL of 0.2% trypsin 0.02% EDTA. DMEM/F-12 medium (25 ml) containing 10% Newborn Calf Serum (NCS) and 1% Pen/Strep was added and the digested tissue was filtered over a gauze mesh. The filtrate was washed and layered on Ficoll for density gradient centrifugation (20 min, 800 g). Cells were collected from the interface, washed and incubated for 20 min at 37°C in a tissue culture dish to remove adherent macrophages. EVT were obtained after sorting for live large CD45^{-} cells or CD45^{-}B7-H3^{+} cells. Sorted cells were plated in 96 or 48 well plates with or without 10 mm coverslips (1.5 mm thick, TedPella Inc) coated with 20 μg/ml fibronectin in EVT medium (see Primary human and mouse cell culture) and non-adherent cells were removed 3-18 h later. Adherent cells were 50%–95% HLA-G^{+} EVT (Crespo et al., 2016; Tilburgs et al., 2015b).

To isolate immune cells, decidual tissue was washed with PBS, minced and digested with 0.25% collagenase type IV and 0.025% DNase I with gentle shaking in a water bath for 75 min at 37°C. Released lymphocytes were washed with RPMI 10% FBS filtered through 100, 70 and 40 μm sieves (BD, Labware; NJ), and the filtrate was resuspended in 20 mL 1.023 g/ml Percoll and layered on a Percoll gradient (10 mL 1.080 g/ml topped with 15 mL 1.053 g/ml) for density gradient centrifugation (25 min/800 g). Lymphocytes were isolated from the 1.080 g/ml/1.053 g/ml interface, washed with RPMI and stained for flow cytometry analysis or sorting of dNK and decidual macrophages using the gating strategy described in Tilburgs et al. (2015b). pNK were isolated using a RosetteSep human NK enrichment cocktail followed by Ficoll density gradient centrifugation (20 min, 800 g). Monocyte-derived macrophages were obtained by isolating peripheral blood mononuclear cells by Ficoll density gradient centrifugation (20 min, 800 g) and culturing overnight in RPMI + 10% FCS without antibiotics. Non-adherent cells were removed, and adherent cells were used as macrophages.

Mouse uNK were isolated as previously described (Zhang et al., 2005). Briefly, the mesometrial lymphoid aggregate of pregnancy and decidua were minced and incubated with collagenase IV for 60 min. Single cell suspensions were subjected to Percoll gradient centrifugation. The uterine leukocyte band at the 40%–80% Percoll interface was collected. Mouse splenocytes were obtained after

mechanical dissociation of spleens and passage through a 70 μm sieve. NK were isolated from uterine leukocytes or splenocytes using an NK cell magnetic purification kit.

Placental villous 3D cultures

Villous trees (2-3 mm length) from 6-9 weeks gestation human pregnancies were dissected and cultured in Transwell inserts (0.4 μm pore, Costar) coated with Matrigel (Rizzuto et al., 2016). Villi were allowed to invade the Matrigel for 12-15 h with collection medium (DMEM/F12 with 2.5% FBS, 1% Pen/Strep, 50 μg/ml gentamicin and 1.25 μg/ml amphotericin) only in the bottom well. For infection, villi were washed with antibiotic-free villous medium (DMEM/F12 with 20% FCS) and cultured in the same medium for 1 h before infection. Cultures were harvested for CFU assay and imaging after 3 d of culture with or without added autologous dNK.

Primary human and mouse cell culture

Human pNK and dNK were cultured in X-VIVO 10^{TM} media without antibiotics supplemented with 5% human AB serum and 2.5 ng/ml recombinant human IL-15 for 12-18 h prior to experiments. Human dMϕ and pMϕ were cultured in RPMI with 10% FCS without antibiotics. Human HLA-G^{+} EVT were cultured in DMEM/F12 medium supplemented with 10% NCS, 1x Pen/Strep, 1x insulin, transferrin, selenium (ITS), 5 ng/ml EGF, and 400 units human gonadotropic hormone as described (Tilburgs et al., 2015a). Murine sNK and uNK isolated from pregnant WT or *GNLY*-Tg mice were cultured in RPMI with 10% FCS without antibiotics supplemented with 2.5 ng/ml recombinant mouse IL-15.

Flow Cytometry

For surface staining, cells were stained for 30 min on ice in the dark in PBS 1% FCS after 5 min incubation with Fc-Block. Cells were analyzed immediately or fixed in 1% paraformaldehyde (PFA) for 10 minutes for next day analysis. For intracellular staining, cells were fixed and permeabilized using the BD CytoFix/CytoPerm kit. Analysis was performed on a FACSCalibur, LSR II or FACSCanto II (BD) using FlowJo Version 10 and sorting was done using a BD Aria II.

Cytolytic proteins in culture supernatants

dNK, pNK, uNK and sNK (2x10^{6} cells/ml) were cultured for 12 h in antibiotic-free X-vivo 10^{TM} with 2.5 ng/ml IL-15. Culture supernatants were collected and snap frozen at −80°C until analysis. GNLY concentration was measured by ELISA. GzmA, GzmB and PFN concentration were measured by Milliplex MAX in a Luminex instrument.

GNLY immunoprecipitation and immunoblot

dNK and pNK supernatants from 12 h cultures (4x10^{6} cells/ml in IL-15-containing medium as described above) and NK lysates were incubated for 1 h with Protein G Dynabeads pre-loaded with 10 μg of anti-GNLY. The precipitates were eluted in NuPage 4x Loading Buffer 0.7% β-ME. JEG-3 were lysed using RIPA buffer with complete protease inhibitor. Lysates from JEG-3, purified GNLY isolated from YT-Indy cells (Thiery et al., 2010) and the IP from NK lysates and supernatants were analyzed by immunoblot probed with goat anti-human GNLY antibody (1:1000) and mouse anti-human β-actin antibody (1:1000).

Imaging Flow Cytometry

Freshly sorted dNK and pNK, or pNK stimulated with 5 ng/ml IL-15 and 50 IU/ml IL-2 for 6 d were fixed and permeabilized using the BD CytoFix/CytoPerm kit, and stained first with anti-GNLY (clone RB1), anti-PFN and anti-GzmB for 20 min, and then with Hoechst 33342 for 10 min. Mitochondria were stained by incubation with 500 nM Mitotracker Deep Red in serum-free medium for 30 min at 37°C, and cells were washed in complete medium, and then fixed and permeabilized using the BD CytoFix/CytoPerm Kit for GNLY staining. Images were acquired using an AMNIS Imagestream X Mark II (Luminex). Approximately 10,000 events were acquired for each cell type from 5-6 donors and analyzed using IDEAS Software. Focused cells were identified by the highest Gradient RMS value in the brightfield channel. Single cells were then identified by gating on cells with intermediate Area and high Aspect Ratio in the brightfield channel. To quantify granule versus cytoplasmic fluorescence, cells staining for Hoechst, GNLY and PFN were analyzed using a spot mask (with a spot to cell background ratio of 5 and a radius of 1) to identify GNLY granules, and an intensity mask to identify the whole cell in the GNLY channel. The spot mask was subtracted from the intensity mask to generate a cytoplasm mask. The fluorescence intensity of the granules and cytoplasm was calculated using the Median Intensity Feature (with subtracted background) in each mask. To assess the co-localization of GNLY with PFN or mitochondria, 400 focused cells co-staining for GNLY and PFN were analyzed using the Bright Detail Similarity Feature, which identifies the brightest elements in the fluorescent channel and calculates a log of the Pearson correlation in each cell. Values of 2-3 are considered correlated.

Bacterial and host cell killing assays

NK were harvested after overnight culture in antibiotic-free X-vivo 10^{TM} with 2.5 ng/ml IL-15. Target cells, except for 1° EVT, seeded overnight in 96 well plates (10,000 HLA-G^{+} enriched cells/well), were infected with *Lm* MOI 5 for 30 min. Primary trophoblasts were infected with *Lm* MOI 20. Infected cells were washed 3 times and then treated with gentamicin (50 μg/ml) for 30 min to kill extracellular bacteria, washed 3 times and then cultured with 10^{5} dNK or pNK in duplicate for 3 h in RPMI 10% FCS, or with 100 μl dNK or pNK overnight culture supernatant (from 2x10^{6} cells/ml) for 3 h. Cell-free *Lm* (10^{4} bacteria/100 μl) were also cultured with the same culture

supernatants or medium for 3 h. For *in vitro* experiments with mouse cells, SM9-1 were seeded, infected with *Lm* at MOI 5 and co-cultured with NK isolated from pregnant mice at indicated E:T ratios. Villous cultures were infected with 1.5×10^8 CFU of *Lm* for 5 h and then washed 3 times with PBS, before adding 1 mL of villous medium containing 50 μg/ml gentamicin and 2.5 ng/ml IL-15, with or without 10^6 autologous dNK. One d later, the medium was replaced (without disturbing dNK) with fresh medium containing IL-15 without gentamicin. Cultures were maintained for 2 additional d with daily medium changes. At harvest, villi were washed with PBS and mechanically dissociated, digested with trypsin (as described for isolating primary trophoblasts) and filtered through 100 μm sieves to obtain a single cell suspension. DNA was extracted from 1/3 of the cells using the DNeasy Blood & Tissue Kit and quantified by measuring absorbance at 260 nm by Nanodrop. The remaining cells were used for colony forming unit (CFU) assay. Intracellular bacterial viability was measured by CFU after hypotonic lysis. Colonies were counted after plating 10-fold serial dilutions on BHI agar plates. Host cell viability, except for primary trophoblasts, was assessed by ^{51}Cr release assay. Primary trophoblasts were trypsinized and stained for HLA-G and CD49f and Zombie Yellow to detect dead cells. The percentage of dead HLA-G$^+$ infected trophoblasts cultured without NK was subtracted from the percentage of dead trophoblasts in dNK co-cultures to determine the percentage of specifically killed cells.

Degranulation assay

dNK or pNK, cultured overnight as above, were co-cultured with 721.221 in a 1:3 E:T ratio or with uninfected or *Lm*-infected confluent JEG-3 in antibiotic free RPMI 10% FCS in the presence of CD107a antibody (250 ng/ml) for 4 h before fixing for 10 min in 1% PFA and staining for surface markers.

Transwell experiments

JEG-3 (10,000 cells/well), seeded overnight in the indicated wells of a 96-well Transwell plate (Corning), were infected with *Lm* (MOI 5) for 30 min and then treated with gentamicin to eliminate extracellular bacteria. dNK or pNK (10^5 cells/well) were then added to the indicated wells; 12 h later, infected JEG-3 in the bottom wells were lysed to count CFU.

GNLY/CFSE/DiO transfer experiments

Target cells (50,000 cells/well in 24-well plates) were infected or not with *Lm* (MOI 5, JEG-3; MOI 20, EVT), and co-cultured with NK at indicated E:T ratios and times before washing away NK and trypsinizing targets. For antibody uptake experiments, dNK were cultured overnight without or with 10 μg/ml GNLY blocking antibody (clone DH10 conjugated with CF647 using Mix-n-Stain kit) or IgG1 AF647^{TM}. DH10-CF647 was also added to JEG-3 and NK cultured separately for 1 hr. For nanotube transfer analysis, DiO or CFSE-labeled NK or JEG-3 (labeled according to the manufacturer's instructions) were co-cultured at a NK:JEG-3 ratio of 10:1 or 1:3 for the indicated times (15-60 min for CFSE, 3 h for DiO). Targets and NK were permeabilized and stained for intracellular GNLY (clone RB1) and GzmB, or not permeabilized for analysis of DH10-CF647 or DiO/CFSE uptake. To identify target cells and separate them from NK, JEG-3 and EVT were first surface-stained for HLA-G, CD45 and CD56. Other target cells were stained for CD45 and CD56 (and also CD14 for dMϕ and pMϕ). Target cells were gated based on size and cell surface staining.

Inhibitor experiments

To inhibit intracellular bacterial killing, NK were cultured overnight ($2x10^6$ cells/ml in IL-15-containing medium as above) in the presence of 10 μg/ml GNLY blocking antibody (DH10) or isotype control, 3 μM brefeldin A or 2 mM EGTA. In some cases, NK or JEG-3 were pre-treated with 2 μM cytochalasin D, 10 μM Dynasore or 200 nM DCI for 30 min. In other experiments, indicated cells were treated with 100 U/ml of α2-3,6,8,9 neuraminidase for 1 h in serum-free RPMI, before adding FCS to stop the reaction. Nocodazole (20 μM) was added at the beginning of NK-target cell co-culture. For all inhibitors (except cytochalasin D, Dynasore, neuraminidase, and DCI, which were toxic for long incubations and were washed before the next step), NK were co-cultured with JEG-3 in the presence of the inhibitors or antibody. For cytochalasin and nocodazole treatments in GNLY transfer and microscopy analysis, NK and JEG-3 were centrifuged at 2000 rpm, 2 min at 4°C, before adding cytochalasin D (2 μM) or nocodazole (20 μM) in HBSS and cells were co-cultured for 15 min or 3 h at 37°C before staining for flow cytometry or microscopy imaging. For antibody blocking of GNLY transfer (detected by flow cytometry), dNK of JEG-3 were pre-incubated with 10 μg/ml blocking antibody for 30 min, and antibodies were still present during dNK:JEG-3 co-culture.

Confocal microscopy, Airyscan and structured illumination super-resolution microscopy

NK were adhered for 1 h onto 1.5 mm coverslips (Tedpella, Inc.) coated with 0.01% poly-L-lysine, fixed with 4% PFA for 10 min and then permeabilized with PBS/0.1% Triton-X for 10 min before staining with conjugated antibodies (anti-PFN, anti-GNLY or respective isotypes). Cells were washed and stained with Hoechst 33342 for 10 min. For imaging NK-target cell interactions, target cells (infected or not with DDAO-Far Red-labeled *Lm* MOI 50-200) were co-cultured on 1.5 mm glass coverslips (previously coated with 20 μg/ml fibronectin) with dNK or pNK (E:T ratio 10:1) for 45-60 min. When indicated, JEG-3 or primary EVT were pre-labeled with 1:10,000 CellTracker Deep Red) and dNK were pre-labeled with 1:1000 Vybrant DiO for 30 min in serum-free RPMI and then washed 3 times before co-culture. Coverslips were fixed with 4% PFA in PBS, blocked with PBS containing 10% BSA for 30 min, and stained with surface antibodies to LFA-1, CD56, CD14, CD49f and B7-H3 when indicated for 1 h. After washing, secondary antibodies were added when necessary for 1 h. For GNLY, PFN and tubulin staining, cells were permeabilized with 0.1% Triton-X and blocked again

with 10% BSA for 30 min, before staining overnight at 4°C or for 2-3 h at RT with the primary antibodies, followed by secondary antibodies when necessary. For actin staining, Rhodamine Phalloidin was added to permeabilized cells for 1 h. DAPI was added for 10 min to permeabilized cells. Cells were mounted in Vinol mounting medium.

Villous organ cultures were fixed in 4% paraformaldehyde for 30 min and dehydrated by immersion in 10% sucrose in PBS for 1 h, followed by 20% sucrose for 1 h and 30% sucrose overnight before embedding in OCT medium for flash freezing. Sections (5 μm) were cut using a cryostat (Microm HM 550, ThermoFisher Scientific) and adhered to positively charged glass slides (Denville). OCT was removed by immersion in 1x PBS and tissue was blocked for 30 min in buffer (1% BSA, 22.5 mg/mL glycine, 0.1% Tween 20 in PBS), and then stained overnight at 4°C with primary antibodies to detect CDH-1 (1:25), HLA-G (20 μg/ml), SDC-1 (1:25) and *Lm* (80 μg/ml) in 1% BSA, 0.1% Tween 20 in PBS. After 3 washes in PBS, slides were stained with secondary antibodies (donkey anti-rabbit AlexaFluor 488^{TM} and donkey anti-mouse AlexaFluor 647^{TM} 1:1000) for 1 h at RT. Samples were counterstained with DAPI and mounted and imaged by fluorescence microscopy. To quantify the distribution of Lm-infected cell types or percentage of each cell type that were infected, EVT were identified as HLA-G^{+}CDH1^{+} cells in the tips of villi with large nuclei, CT were CDH-1^{+} cells with smaller nuclei located under ST or EVT and ST were SDC-1^{+} cells with very small nuclei forming a uniform layer on the outside of the villi. Cells were counted in 10 imaging fields (217x magnification).

Imaging of NK (Figures 1D and S1C) and dNK interacting with *Lm*-infected JEG-3/HFF/HeLa/pMϕ (Figures S3A–S3D) was performed using a Zeiss LSM 700 point scanning confocal (Carl Zeiss) with a 63x (1.4NA) oil immersion objective. Lasers were excited at 405, 488, 640 nm with emission filter ranges of 430/90, 500/30, and 650 long-pass, respectively. Images were processed using Zen Blue Lite 2.0. For imaging nanotube connections, some slides (Figure S4A) were imaged in an Olympus FV1000 4-channel Confocal Imaging system coupled to an Olympus IX 81 inverted microscope using a 60x (1.2 NA) water immersion objective. Lasers were 405 nm, 488 nm, 559 nm and 635 nm with emission filters of 425-475 nm, 500-545 nm, 575-620 nm and 655-755 nm, respectively. Images were processed using FV10-ASW software version 03.00.01.15. Nanotube images were obtained using an ELYRA super-resolution microscope (Carl Zeiss) (Figures 5 and 6) with laser lines SIM/PALM/STORM of 405, 488, 561, and 642 nm and a 63x (1.4 NA) oil immersion objective. Super-resolution images were processed using structured illumination to enhance image detail using Zen Blue 2.0. Figures S4F and S4G were obtained with a ZEISS 880 FAST AIRYSCAN laser scanning confocal with laser lines of 405, 488, 561 and 633nm (emission filters of 450, 516, 595 and 654, respectively) and a 63x 1.4NA oil immersion objective. Images were processed using Airyscan processing to enhance image detail with Zen Blue 2.0.

To quantify contacts and nanotube connections (Figures 6A, 6C, 6E, bar plots, S4B–S4E, and S5B and S5E) and image villous cryosections (Figure 3D), slides were imaged using an inverted, fully motorized Axio Observer spinning disk confocal microscope (Carl Zeiss Microimaging, Inc., Thornwood, NY) equipped with a cooled electron multiplication charge-coupled device (CCD) camera with 512 × 512 resolution (QuantEM, Photometics, Tucson, AZ) and a CSU-X1 spinning disc (Yokogawa Electric, Tokyo, Japan) with lasers that were excited at 405, 488, 561 and 640 nm (Coherent, Santa Clara, CA) and emission filter ranges of 452/45, 525/50, 607/36 and 680 long-pass, respectively (Semrock, Rochester, NY). Images were processed using SlideBook V5.0.

Videomicroscopy of dNK-JEG-3 interactions

JEG-3 were cultured in Delta T dishes (Bioptechs) coated with fibronectin (20 μg/ml), which were adapted to an Olympus FV1000 4-channel Confocal Imaging system. dNK were pre-labeled with Vybrant DiO at 1:1000 for 30 min in serum-free RPMI and then washed 3 times. After temperature calibration (37°C), the JEG-3 Delta dish was placed in the stage, and dNK were added at T = 0. Cells were imaged with the 60x objective with transmitted light and 488 nm laser with emission filter of 500-545 nm, and images were taken every minute for up to 20 minutes. Images were processed using FV10-ASW software version 03.00.01.15.

Mouse *in vivo* experiments

On g.d. 6, mice were intraperitoneally infected with exponential phase *Lm* (10^3) in 0.2 mL PBS. Liver, spleen, placenta and fetus were harvested 3 d post-infection, weighed and homogenized in water with 0.2% Triton X-100 for plating on BHI agar plates to assess CFU. Other groups of infected pregnant mice were monitored to term and viable pups were counted. In some experiments, WT or *GNLY*-Tg BALB/c mice were injected intraperitoneally daily for 3 d beginning 3 d before infection (g.d. 3) and weekly thereafter with antibodies to deplete CD4 T cells (0.5 mg/mouse), CD8 T cells (0.5 mg/mouse) or NK cells (0.2 mg/mouse). Control mice received rat IgG2b. Cell depletion was verified by flow cytometry on g.d. 6: blood was collected from the orbital plexus before sacrifice. Spleens were mechanically dissociated and passed through a 70 μm sieve. Livers and uteri were minced and digested with 2mg/ml collagenase D (plus 0.1 mg/ml DNase I) for 45 min. or 0.25mg/ml collagenase IV (plus 0.025 mg/ml DNase I) for 75 min., respectively, before passing through a 100 μm sieve. Blood and tissues were subjected to red blood cell lysis before staining for flow cytometry.

QUANTIFICATION AND STATISTICAL ANALYSES

Values presented are the mean ± s.e.m or median ± interquartile range, as indicated. Statistical analysis was performed using Prism 6.0c (GraphPad). For normal distributions, paired or unpaired ANOVA followed by Tukey post-tests (for multiple comparisons) or paired/unpaired t tests were used. For non-normal distributions, unpaired or paired non-parametric one-way analysis of variance (Kruskal-Wallis test or Friedman's test followed by Dunn's post-test) were used in experiments for which multiple comparisons

were made. To compare 2 groups in experiments with human samples/animals, Mann-Whitney or Kolmogorov-Smirnov tests were used for unpaired groups with equal or unequal variances, respectively. Equality of variances was tested by Levene's test. For paired comparisons of 2 groups, Wilcoxon rank sum test was used. χ^2 test was used to analyze the data where indicated. Non-parametric tests were used in most experiments with human or animal samples because these data were not normally distributed. The statistical method applied to each panel is specified in the legends. $p < 0.05$ was considered significant. None of the experiments were blinded.

Supplemental Figures

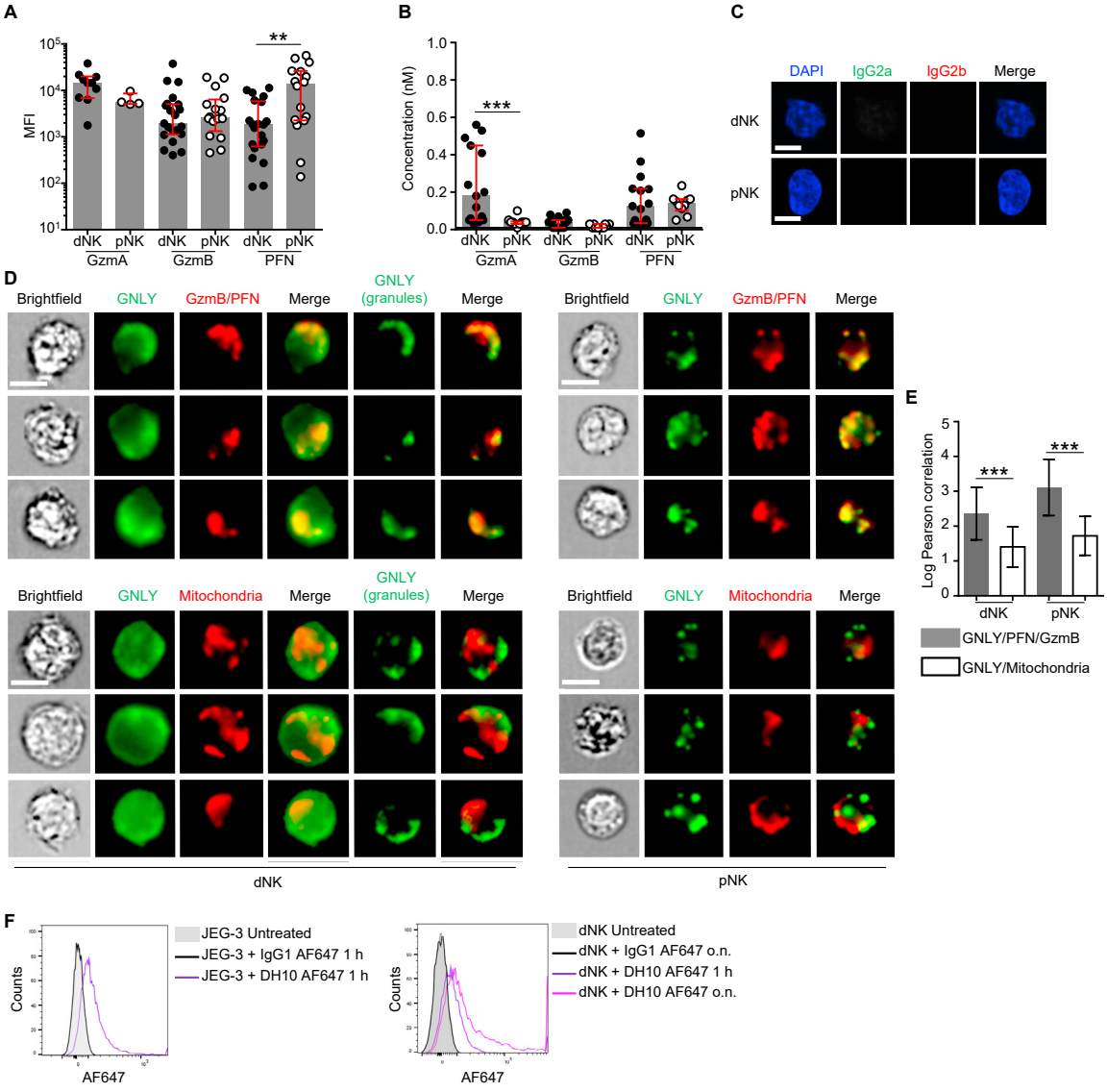

Figure S1. Related to Figures 1 and 2

dNK highly express GNLY, PFN and Gzms.

(A) Mean fluorescence intensity (MFI) of GzmA, GzmB and PFN staining of human dNK and pNK by flow cytometry.

(B) GzmA, GzmB and PFN in 12 h culture supernatants of human dNK and pNK measured by Luminex.

(C) Lack of background staining for GNLY and PFN in Figure 1D using isotype control antibodies. Representative images of dNK and pNK stained with the isotype controls for GNLY RB1 AF488 and PFN dG9 AF647, respectively. Images were acquired with a Zeiss LSM 700 microscope. Scale bars, 5 μm.

(D) Representative raw images from imaging flow cytometry of dNK (*left*) and pNK (*right*) stained for total GNLY (RB1) and PFN and GzmB (*top*) or MitoTracker (*bottom*). dNK "GNLY granules" images were edited to remove cytoplasmic brightness to enhance the granules. Scale bars, 7 μm.

(E) Log of Pearson correlation of GNLY/PFN granule staining, and GNLY granule/Mitotracker staining. 400 cells from one dNK donor and one pNK donor were analyzed using the Bright Detail Similarity Feature from IDEAS software, comparing GNLY granules with PFN granules and GNLY granules with mitochondria.

(F) JEG-3 and dNK take up GNLY antibody from the medium when incubated at 37°C. Representative flow cytometry plots showing the uptake of AF647-labeled isotype control or GNLY blocking antibody (clone DH10) by JEG-3 (*left*) or dNK (*right*) after 1 h or overnight incubation (o.n.) at 37° C. The histograms are representative of 3 donors.

Bars represent median ± interquartile range (A, B) and mean ± s.e.m. (E). **p < 0.01, ***p < 0.001 by Mann-Whitney rank test or Kolmogorov-Smirnov test (A,B) or paired t test (E).

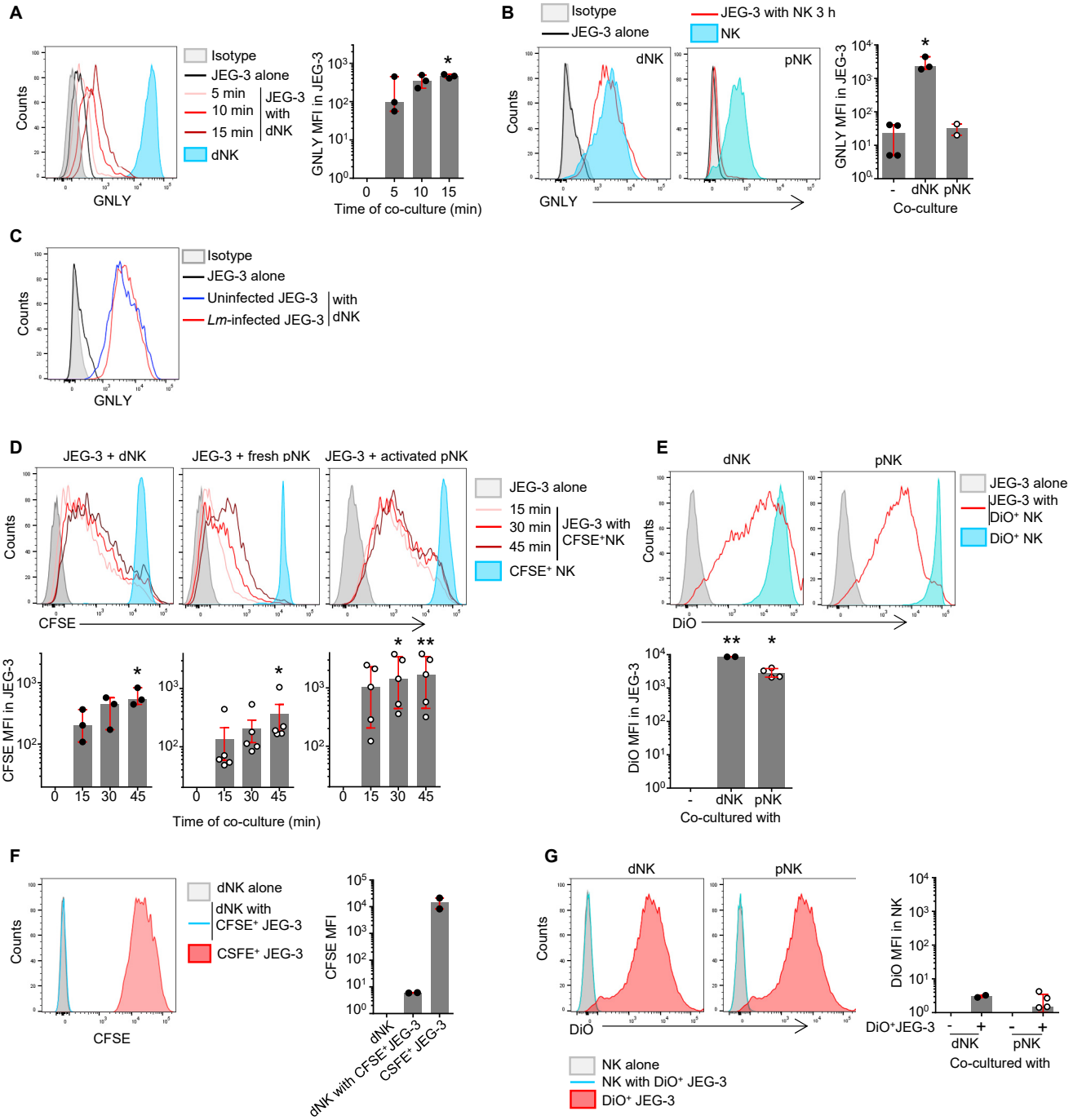

Figure S2. GNLY Transfer from dNK to JEG-3 Cells Is Detected within 5 Min of Co-culture and Is Independent of Infection, and dNK Cells Transfer Small Dyes to JEG-3 Cells Unidirectionally, Related to Figure 4

(A) Representative flow cytometry histograms (*left*) of NK and JEG-3 with or without co-culture with dNK for the indicated times. Shown in the graph (*right*) is GNLY MFI in JEG-3 after subtracting background staining without added dNK.

(B) Representative flow cytometry histograms (*left*) and change in GNLY MFI (*right*) in NK and JEG-3 after co-culture with dNK or pNK for 3 h.

(C) Representative flow cytometry histograms of intracellular GNLY staining in uninfected or *Lm*-infected JEG-3 that were cultured with or without dNK for 3 h.

(D) Representative flow cytometry histograms of CFSE fluorescence in NK or JEG-3 (*top*) after culture with or without CFSE-labeled dNK (*left*), freshly isolated pNK (*middle*) or pNK activated with cytokines for 6 days (*right*) for the indicated times. Graphs (*bottom*) shown median CFSE MFI transferred from each type of CSFE-labeled NK over 45 min.

(E) Representative flow cytometry histograms (*top*) and DiO MFI (*bottom*) in DiO-labeled NK and JEG-3 cultured for 3 h with or without labeled NK.

(legend continued on next page)

(F) Representative flow cytometry histogram (*left*) of JEG-3 and dNK that were cultured with or without CFSE-labeled JEG-3 for 1 h (NK:JEG-3 ratio 3:1) and median CFSE MFI in the cells from 2 co-cultures (*right*).

(G) Representative flow cytometry histograms (left) and DiO MFI in DiO-labeled JEG-3 and NK cultured for 3 h with or without labeled JEG-3.

Graphs show median ± interquartile range. $p < 0.05$; $^{**}p < 0.01$ by paired non-parametric one-way ANOVA (Friedman's test followed by Dunn's post-test compared to time 0 (A, D)), unpaired non-parametric one-way ANOVA (Kruskal-Wallis test followed by Dunn's post-test of each NK type compared to control (B, E)), and Wilcoxon rank sum test (F, G).

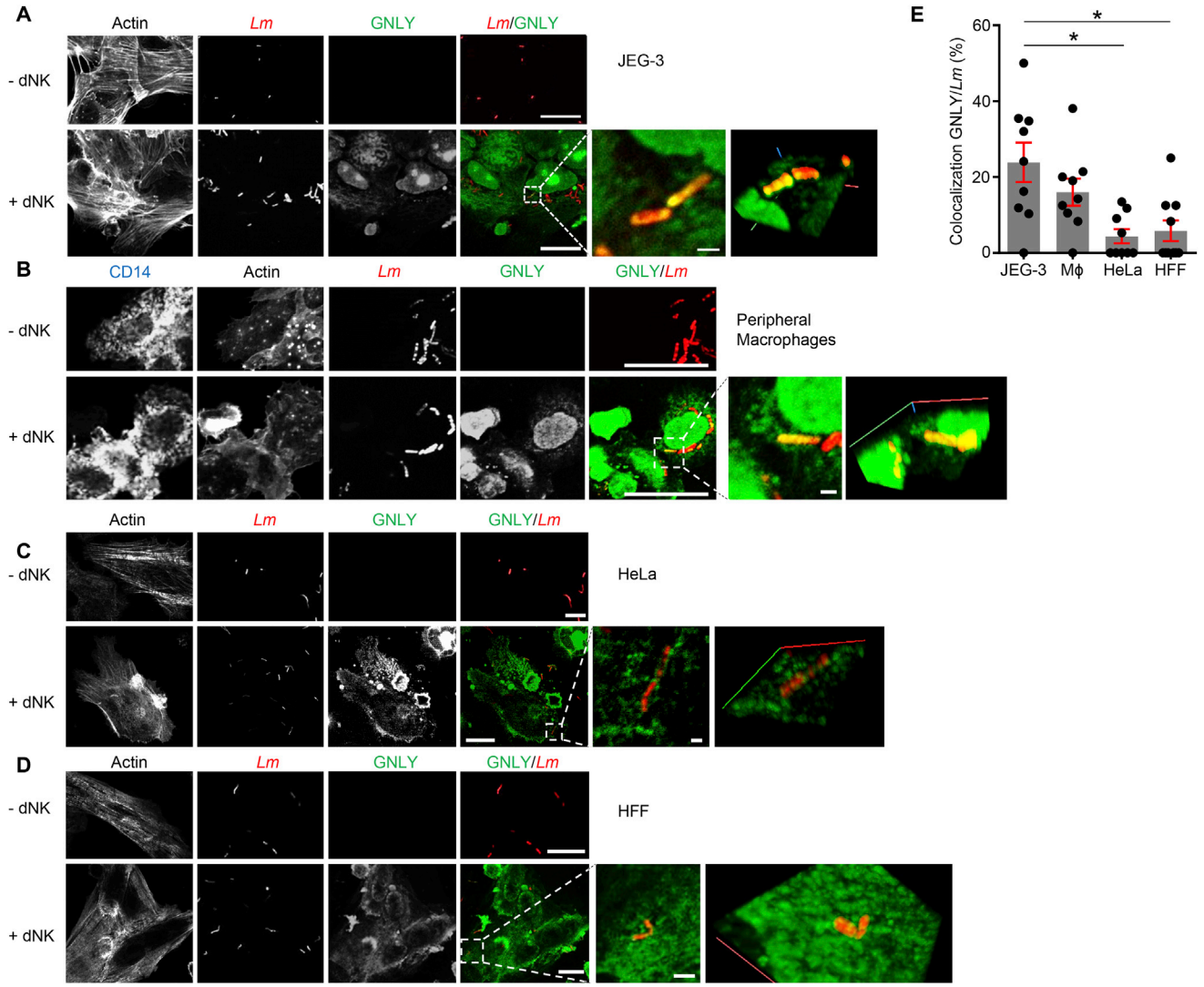

Figure S3. GNLY Transferred from dNK Cells Co-localizes with *Listeria* in JEG-3 Cells and Macrophages, Related to Figure 4

(A-D) Representative confocal microscopy images showing colocalization of GNLY (green – clone RB1) with *Lm* (red) in JEG-3 (A), pMϕ (B), HeLa (C) and HFF (D) before *(top)* and after *(bottom)* 1 h co-culture with dNK. The rightmost images show 3D representations of the inserts. Images were obtained with a Zeiss LSM 700 microscope. Scale bars: left, 20 μm; right (insert): 1 μm.

(E) Percentage of *Lm* showing GNLY stain in indicated target cells, observed in 10 fields (each dot represents one field). Graph shows median ± interquartile range (E). *$p < 0.05$ by unpaired non-parametric one-way ANOVA (Kruskall-Wallis test) followed by Dunn's post-test, comparing each cell target with each other.

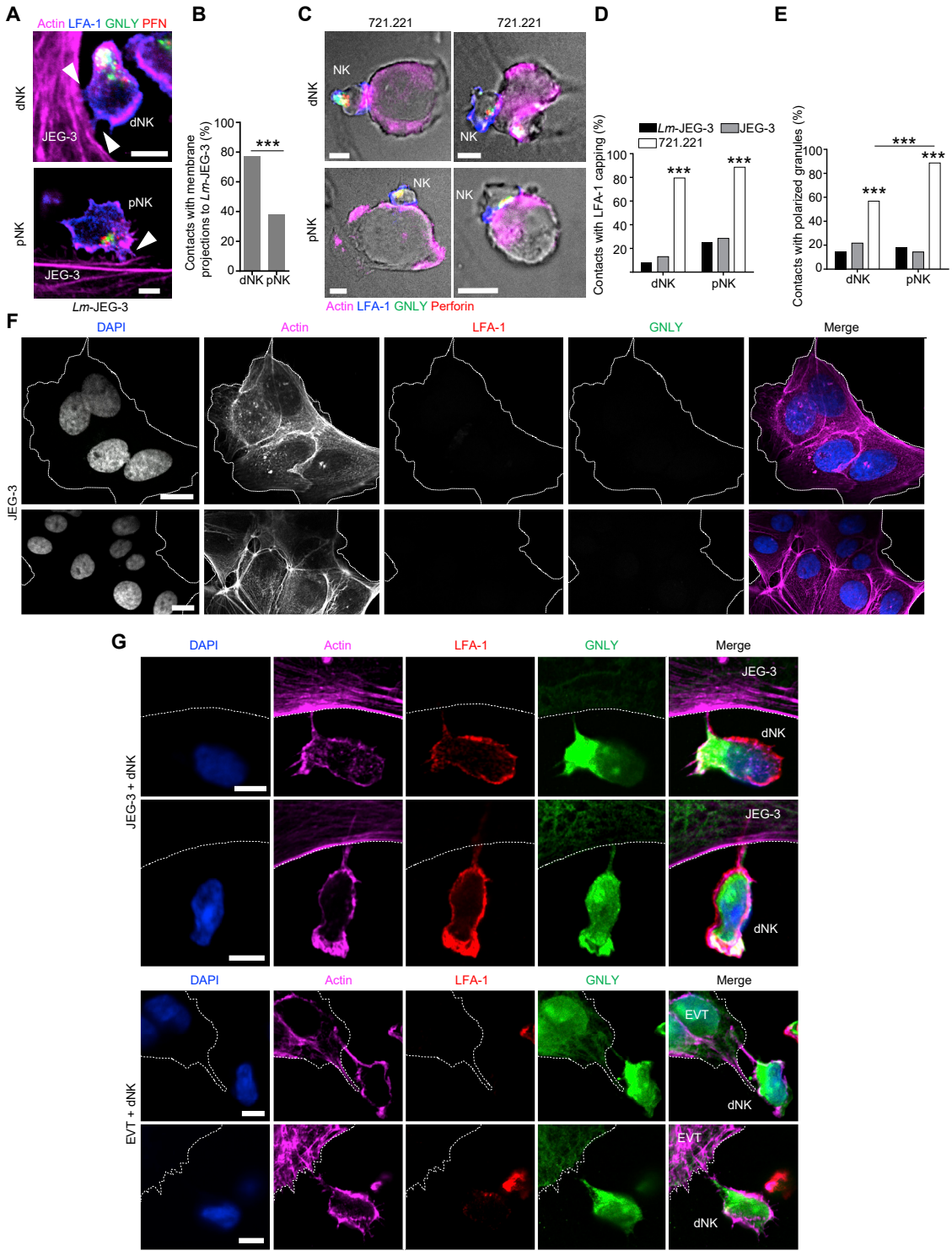

Figure S4. NK Cell Contacts with Target Cells, Related to Figure 5

(A) Representative confocal images of dNK and pNK contacts with *Lm*-infected JEG-3 stained for GNLY (clone RF10) (green), PFN (red), LFA-1 (blue) and actin (magenta). Scale bars: 5 μm. Images with uninfected JEG-3 were similar (not shown). Co-culture lasted 45 min. Images were obtained with an Olympus FV1000 microscope.

(B) Percentage of dNK and pNK in contact with Lm-infected JEG-3 displaying cytoplasmic connections. For each condition, at least 44 dNK and pNK contacts from one donor each were analyzed, and the percentage of these contacts where membrane projections were observed was calculated.

(legend continued on next page)

(C) Representative fluorescence microscopy images of dNK and pNK contacts with 721.221. dNK and pNK contacts with 721.221 without granule polarization to the immune synapse are shown on the left, while contacts with granule polarization are shown on the right. Images were acquired with the Axio Observer spinning disk confocal microscope. Scale bars, 5 μm. Co-culture lasted 45 min.

(D, E) Percentage of dNK and pNK contacts with indicated target cell that show LFA-1 capping (D) or granule polarization to the area of intercellular contact (E). χ^2 test compared NK interactions with uninfected and infected JEG-3 and 721.221 from the same representative donor. 45 NK-target contacts were counted for each target.

(F) Representative single channel and merged images of JEG-3 cultured alone and stained for actin (magenta), GNLY (green) and LFA-1 (red). JEG-3 membrane is delineated. Scale bars: 20 μm.

(G) Representative single channel images (obtained using a ZEISS Airyscan 880) showing GNLY (RB1 - green) in the target cells and in the cytoplasmic connections (actin, magenta) and between dNK and JEG-3 or 1° EVT co-cultured for 60 min. LFA-1 (red) is only expressed in dNK. JEG-3 and EVT cell membranes are outlined in white. GNLY is visible within target cells. Scale bars, 5 μm. ***$p<0.001$ by χ^2 test (B, D, E).

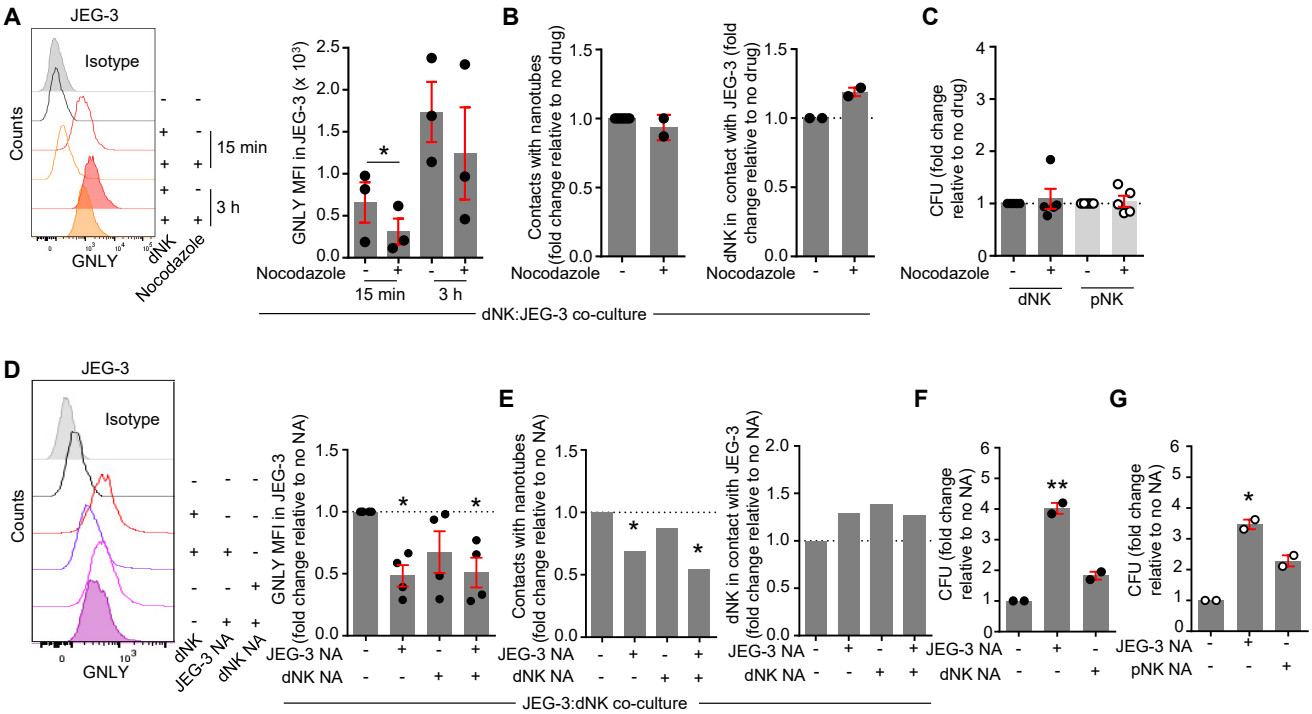

Figure S5. GNLY Transfer, Nanotube Formation, and *Lm* Suppression by NK Cells Depend on Sialylation of Target Cell Ligands but Not on Microtubules, Related to Figure 6

(A) Representative flow cytometry histograms of intracellular GNLY staining (*left*) and GNLY MFI (*right*) in JEG-3 cultured with dNK (E:T ratio 3:1) for 15 min or 3 h, in the presence or absence of nocodazole. Shown at right are median ± interquartile range of 3 donors.

(B) Effect of nocodazole on the proportion of dNK:JEG-3 contacts with visible nanotube connections (*left*) and on the proportion of NK in contact with JEG-3 (*right*) after 15 min co-culture. Shown is fold change compared to no nocodazole (mean ± s.e.m). For each condition, at least 24 dNK:JEG-3 contacts using dNK from 2 donors were analyzed.

(C) Effect of nocodazole on NK suppression of intracellular *Lm* CFU in JEG-3 after 3 h. Shown are mean ± s.e.m fold change relative to co-culture with NK without nocodazole in 5 donors.

(D-G) Effect of neuraminidase (NA) pre-treatment of dNK or JEG-3 on GNLY transfer from dNK to JEG-3 (D), percentage of dNK:JEG-3 cell contacts with visible nanotube connections (*left*) and percentage of dNK in contact with JEG-3 (*right*) (E), and on change in bacterial CFU (mean ± s.e.m). after incubation with dNK (F) or pNK (G) in 2 donors each. (D) shows representative flow cytometry histograms (*left*) and median ± interquartile range of fold change in GNLY MFI (*right*) in JEG-3 co-cultured with dNK. In (E), at least 30 dNK:JEG-3 contacts in one donor were analyzed for each condition. *$p < 0.05$, **$p < 0.01$, Wilcoxon rank sum test (A, C), χ^2 test (B, E) and paired non-parametric one-way ANOVA (Friedman's test followed by Dunn's post-test), comparing each treatment with no inhibitor control (D, F, G).

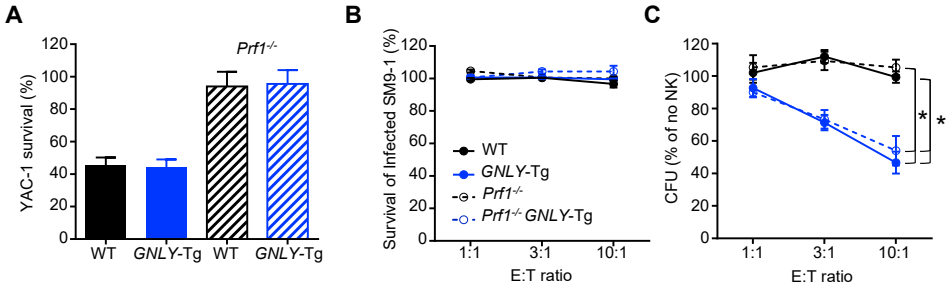

D

		Tissue and antibody used for depletion															
		Blood				Spleen				Liver				Uterus			
Gate	Lymphocyte	Isotype	NK	CD8	CD4	Isotype	NK	CD8	CD4	Isotype	NK	CD8	CD4	Isotype	NK	CD8	CD4
CD45+	NK, %	15	0.1	12	16	5	0.2	3.8	5	10	0.9	9	9	13	2	12	20
CD45+CD3+	$CD8^+$ T, %	28	20	0	85	28	23	0.3	65	18	11	0	50	13	6	0	27
	$CD4^+$ T, %	69	78	99	0.8	68	73	95	0.2	70	78	84	1	69	77	85	8

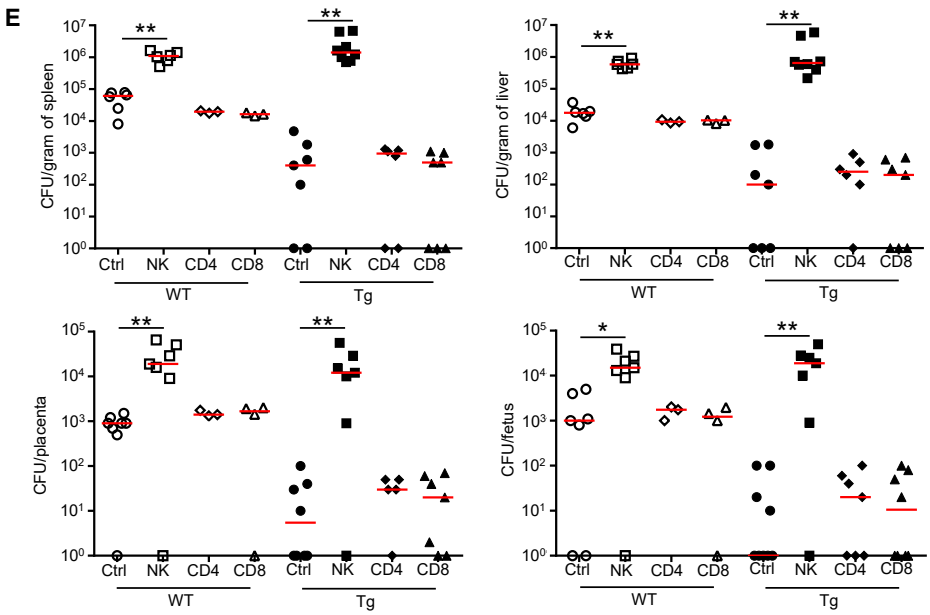

Figure S6. *GNLY*-Tg Mouse NK Cells Kill Intracellular *Lm* Independent of PFN and Are the First Line of Defense against *Lm*, Related to Figure 7

(A-C) Viability of YAC-1 (A) and infected SM9-1 (B) and intracellular *Lm* CFU in SM9-1 (C) after co-culture for 3 h with uNK from pregnant WT, *Prf1*$^{-/-}$, *GNLY*-Tg or *Prf1*$^{-/-}$*GNLY*-Tg mice (3 mice/group). Shown are mean ± s.e.m.

(D) NK and T lymphocyte depletion in pregnant mice. Values show percentages of the different subsets after each antibody depletion. Blood and tissue were obtained on g.d. 6 (1 WT mouse per condition).

(E) Bacterial CFU on g.d. 9 in WT and *GNLY*-Tg mice that were depleted of lymphocyte subsets using control antibody (Ctrl) or NK, CD4 or CD8 depleting antibodies on g.d. 3 and then infected with *Lm* on g.d. 6 (n = 3-8 mice/group) Red lines represent the median. *$p < 0.05$, **$p < 0.01$; by unpaired non-parametric one-way ANOVA (Kruskal-Wallis test (A-C) followed by Dunn's post test comparing each transgenic mice group with WT (A) and area under the curve (B,C)); and non-parametric unpaired one-way ANOVA (Kruskal-Wallis followed by Dunn's post-test), comparing each group with respective control (E).